A Review of Fractal Conductance Fluctuations in Ballistic Semiconductor Devices

Chapter appearing in: Electron Transport in Quantum Dots

Richard Taylor[1]*, Richard Newbury[2], Adam Micolich[2], Mark Fromhold[3], Heiner Linke[1], Giles Davies[4], Jon Bird[5], Theodore Martin[1] and Colleen Marlow[1]

1. *Department of Physics, University of Oregon, Eugene, OR 97403-1274, U.S.A.*
2. *School of Physics, University of New South Wales, Sydney, 2052, Australia.*
3. *School of Physics and Astronomy, Nottingham University, Nottingham NG7 2RD, U.K.*
4. *Cavendish Laboratory, Cambridge University, Cambridge, CB3 OHE, U.K.*
5. *Center for Solid State Research, Arizona State University, Tempe, AZ 85287-6206, U.S.A.*

*Email: rpt@darkwing.uoregon.edu, Fax: 1-541-346-3422, Tel: 1-541-346-4741

Contents:

1. Introduction

The ability to scale device sizes to below a micro-meter has profound implications for electron conduction in semiconductor systems. For conventional circuits, the reduced component size offers the rewards of higher packing densities and faster operating speeds. However, in terms of the search for new classes of electronic devices, designed to replace the transistor as the basic component of electronic circuits, the prospect of current flow across sub-micron distances holds even greater potential. Traditional current flow concepts, in which electron propagation along the device's length is modelled as a classical diffusion process, can no longer be applied. Both the classical and quantum mechanical transmission characteristics may ultimately be harnessed to produce revolutionary modes of device functionality. Intimately coupled to these objectives of applied physics, sub-micron devices also provide a novel environment for the study of a rich variety of fundamental semiconductor physics.

Fuelled by these considerable goals, many techniques for constructing sub-micron devices have emerged over the last twenty years. One of the more successful approaches adopts the cornerstone of the microelectronics industry – metallic surface patterns - and reduces their length scales through the use of electron-beam rather than optical lithography.[1-3] In particular, since its first demonstration in 1986,[4] surface gates have frequently been used to define corresponding patterns in the two-dimensional electron gas (2DEG) at the interface of AlGaAs/GaAs heterostructures.[1] Whereas this 'top-down' construction technique (where component devices are formed within a macroscopic material) can routinely define devices with feature sizes of 50nm, more recent 'bottom-up' technologies (where atomic components are assembled to form a device), are capable of constructing even smaller device sizes. Nevertheless, the gated AlGaAs/GaAs system remains successful due to its capacity to define small devices in the high quality environment provided by the host semiconductor material. In particular, surface gate technology remains the technique of choice for studies of 'ballistic' electron conduction, where the device size is smaller than the average distance ℓ between scattering sites in the material.

When first observed in 1988,[5, 6] the appeal of the ballistic conduction regime was thought to lie in its remarkable simplicity: through the use of sophisticated semiconductor growth and lithography techniques, devices could be constructed in which the electrons were unhindered by material-induced scattering events.[1, 7] The electrons followed straight trajectories, allowing experiments originally planned for vacuum to be performed in a solid-state environment! A famous example of this concept is the semiconductor 'billiard'. Analogous to a billiard table, electrons in the 2DEG move along a two-dimensional plane bounded by shaped walls. Because the bounded region is smaller than ℓ, electrons passing between the entrance and exit (formed by openings in the walls) follow ballistic trajectories shaped predominantly by the walls (see Fig. 1(a)). In the early 1990s, experimental[8, 9] and theoretical[10, 11] research focussed on a comparison of two distinct billiard shapes – stadia and circles. The reasoning behind this choice was that circular cavities were expected to produce stable trajectories, whilst the combination of curved and straight walls of the stadium would generate chaotic electron trajectories exhibiting an exponential sensitivity to initial conditions.[12] Furthermore, these ground-breaking studies moved beyond classical chaos by investigating 'quantum chaos' - the quantum mechanical behavior of the classically chaotic electrons.[13]

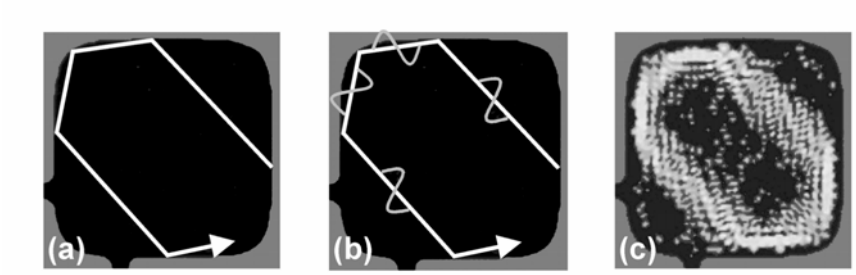

Figure 1 (a) A schematic representation of a classical electron trajectory within a billiard. (b) In the semi-classical regime, electron waves travel along the trajectories. (c) A simulation showing the intensity variation of a quantum wave.

This exploration of quantum chaos in electronic conduction serves as the starting point for the experiments presented in this chapter. In our experiments, the semiconductor billiards are cooled to milli-Kelvin temperatures to reduce the electron scattering events (for example, with phonons and other electrons) that disrupt the coherence of the electrons' quantum mechanical wave properties. When the electrons reach a temperature of 30mK, the characteristic phase-coherence length of the waves is in excess of 30μm, allowing electrons to maintain coherence whilst traversing billiards with

typical sizes of 1μm. Traditionally, this billiard size is regarded as optimal for studies of quantum chaos. Whilst being sufficiently small to ensure phase coherence and therefore that the quantum wave-character of the electrons plays a crucial role in the conduction process, it also ensures that the ratio S of the billiard size to the electron Fermi wavelength (~50nm) is relatively large. Electron transport within the billiard is then semi-classical rather than fully quantum-mechanical. A crucial consequence of the semi-classical regime is that the electron waves can be pictured as moving along the classical trajectories (see Fig. 1(b,c)).[7, 10, 11] As they do so, the waves accumulate phase and this determines the wave interference between pairs of trajectories that intersect to form closed loops.[7] This interference process can be investigated experimentally by tuning the phase through the application of a small magnetic field B perpendicular to the plane of the billiard.[7] According to the Aharonov-Bohm effect, each loop generates a periodic oscillation in the conductance with a magnetic field period ΔB inversely proportional to area enclosed by the loop.[7, 14] Because a typical billiard supports a distribution of loop areas, the magneto-conductance $G(B)$ is composed of oscillations with many different periods. The resulting fluctuations can then be viewed as 'magneto-fingerprints' of the classical trajectories because they are sensitive to the precise, microscopic distribution of loop areas in the billiard.[8, 9, 15] In this way, the underlying classical chaos in the trajectories is expected to manifest itself in the quantum behavior of the billiard - that is, quantum chaos.

We find that patterns observed in the magneto-conductance fluctuations repeat at increasingly fine magnetic field scales, a phenomenon that has since been labelled as fractal conductance fluctuations (FCF).[16] Furthermore, two distinct forms of fractal behavior are observed – exact self-affinity (where the patterns observed at increasingly fine field scales repeat exactly) and statistical self-affinity (where the patterns simply follow the same statistical relationship at different scales). Statistical self-affinity describes many of nature's patterns, ranging from clouds to coastlines.[17, 18] In contrast, although exact self-affinity has been the subject of mathematical studies for over one hundred years, observations of this form of fractals in physical systems remain rare.[17, 18] The billiards investigated therefore represent a unique physical environment in which both forms of fractal can be observed. Furthermore, fractal studies in natural

environments are ‘passive’ in the sense that there is no experimental interaction with the system being investigated. In contrast, the semiconductor billiard represents an artificial environment in which the conditions can be controlled and adjusted in a systematic fashion. We exploit this control to address fundamental questions about transitions in fractal behavior. In particular, we investigate how fractal behavior evolves between its two distinct forms (exact and statistical self-affinity) and also how fractals deteriorate into non-fractal behavior as the process generating them is gradually suppressed. These central issues cannot be addressed using other physical systems and this unique opportunity has generated considerable interest from the fractals and chaos research communities.

The primary motivation for this research, however, remains firmly anchored in semiconductor physics and the exploration of electron conduction properties of sub-micron electronic devices. Almost fifteen years on from the first observation of ballistic conduction in semiconductor devices, their basic properties are not as simple as initially hoped. Despite the continued use of the descriptive title of 'billiard', these devices do not follow the well-understood rules of their name-sake! Magneto-conductance measurements play a central role in many studies of sub-micron semiconductor physics, yet there is no theoretical basis for the observed fractal behavior. In contradiction to initial expectations and theory, fractal conduction fluctuations are not restricted to the semi-classical conduction regime. Instead, they appear to be a generic feature of ballistic conduction in small devices, extending across the spectrum of classical, semi-classical and quantum conduction regimes.

Far from trivial, this preservation of fractal character is quite remarkable. Fractals are a holistic phenomenon: if the contribution of just one trajectory loop is changed, then *all* the other loops supported by the billiard have to adjust in order to preserve the fractal scaling properties of the conductance. In this sense, fractal conductance fluctuations are a sensitive probe of the underlying dynamic properties of *all* the ballistic trajectories determining the conduction process. In this chapter, we will present a review of the experimental quantification of this fractal phenomenon, along with recent and surprising experimental developments, in the hope that these novel

observations will attract further theoretical interest in the relationship between the fractals and the chaotic dynamics that generate them, leading to an improved understanding of electron conduction processes at the sub-micron scale.

2. The Semiconductor Sinai Billiard: can Chaos be Controlled with the "Flick of a Switch?"

We began our investigations in 1994 with the question, "can chaos be controlled with the flick of a switch?" Two years earlier, the experiment that pioneered the study of quantum chaos in semiconductor billiards had detected a significant difference in the magneto-conductance fluctuations generated by two billiards – one was a circular billiard designed to support stable trajectories, the other a stadium designed to support chaotic trajectories.[8] A natural step forward in these investigations would be to see if the same effects could be observed in a *single* device: could the billiard parameters be adjusted to introduce or remove chaotic dynamics from the quantum conduction process? At this time, the semiconductor community was eagerly exploring analogies between ballistic electrons and ray optics, where electrostatic surface gates were being used to 'steer' ballistic trajectories through reflection, refraction or collimation.[7] We therefore proposed the idea of a 'hybrid' billiard where certain sections of the billiard wall would be shaped to support stable trajectories whilst others would have curved surfaces designed to diverge the trajectories and generate chaotic sensitivity. The ballistic beam injected into the billiard could then be directed to either the chaotic or stable region of the billiard by tuning the voltage applied to a 'steering' gate. In the experiment that evolved from this principle, chaos was introduced into the quantum conduction by directing a collimated beam of electrons at the curved surface located around the exit of the billiard.[19] Evolving this principle further still, rather than deflecting beams from straight to circular walls, why not introduce the chaos by inserting a circular object into the flow of ballistic trajectories?

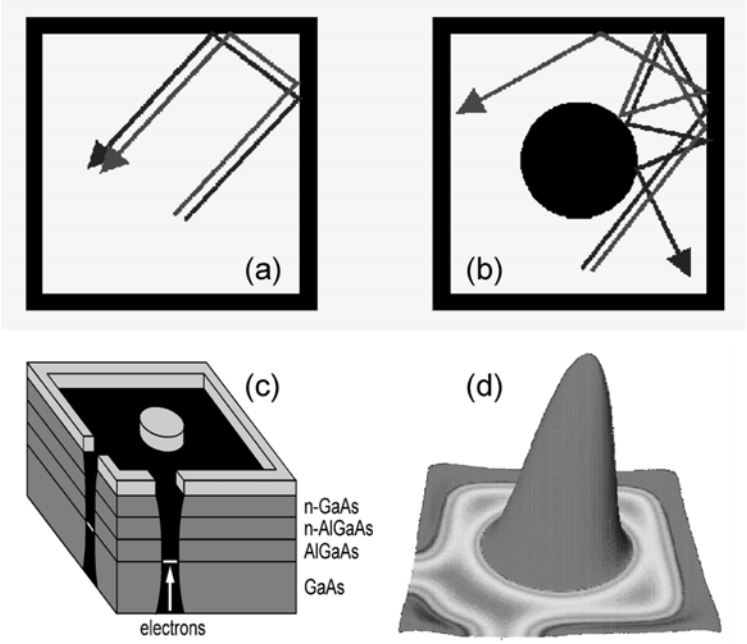

Figure 2 (a) Two electron trajectories launched with similar initial conditions. Shaped by collisions with the square billiard, these stable trajectories do not diverge significantly. (b) In contrast to the square billiard, the same two trajectories rapidly diverge in the Sinai billiard due to scattering events with the circle. (c) A schematic representation of the surface gate technique used to define the Sinai billiard in the 2DEG located below the surface at the AlGaAs/GaAs interface. The light grey regions indicate the depletion regions under the gates. (d) Self-consistent calculations of the soft-wall potential landscape expected for the Sinai billiard defined by surface gates. Potential energy (vertical axis) is plotted as a function of position within the billiard.

The very same idea had been explored mathematically twenty-five years earlier by a Russian chaologist called Sinai.[20] Sinai presented a theoretical investigation of the trajectories of classical particles and how collisions with straight and curved walls affected the dynamics of the particles. In particular, the geometries shown in Fig. 2(a,b) have since become a model system for the theoretical demonstration of chaotic trajectories. Whereas the 'empty' square billiard shown in Fig. 2(a) supports stable trajectories, introduction of the circle at its center transforms the geometry into the so-called Sinai billiard shown in Fig. 2(b). This simple transition has a profound effect on the billiard's scattering dynamics. The convex surface of the circular scatterer acts as a 'Sinai diffuser' producing diverging trajectories, whilst the straight outer walls bounce the trajectories back towards the diffuser to repeat the diverging process over and over. The result is to produce trajectories with an exponential sensitivity to initial conditions - the signature of chaotic behavior.[12, 20]

Possible systems in which this elegant method for generating chaos could be achieved include microwave cavities,[21] atom optics[22, 23] and semiconductor billiards. The most flexible construction technique for semiconductor billiards is shown in the schematic representation of Fig. 2(c). Within the semiconductor heterostructure shown, a 2DEG is located at the interface between the GaAs and AlGaAs layers. The billiard is defined in this 2DEG using the patterned metallic gates (light grey) deposited on the heterostructure surface. A negative gate bias defines depletion regions (medium grey), forming the billiard walls in the regions of the 2DEG directly below the gates.[1, 7] In contrast to the physical walls of microwave cavities, these electrostatic walls can be switched on and off and their sizes varied by tuning the gate bias, allowing an evolution in the billiard geometry. In particular, the central circle can be switched off, allowing the transition from the Sinai billiard to the empty square shown in Fig. 2(a,b).

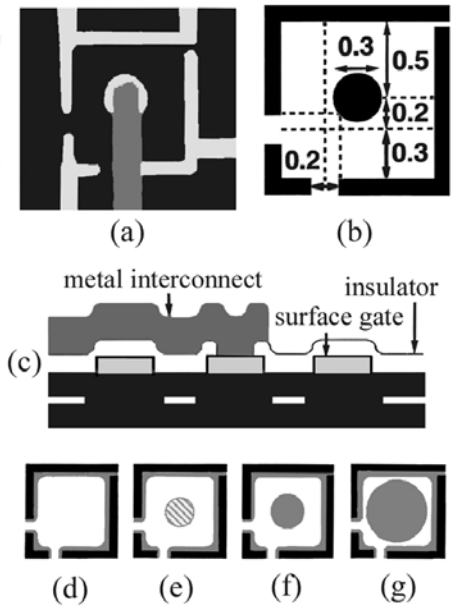

Figure 3 (a) A scanning electron micrograph of the Sinai billiard device. (b) A schematic representation of the surface gate geometry. The lithographic dimensions are in microns. The dashed lines are guides indicating the relative position of the central gate. (c) A cross-section showing the bridging interconnect that traverses the billiard above a thin layer of insulator. The bridge contacts to the central circular gate through a hole etched in the insulator in the region directly above the central gate. (d)-(g) Schematic representations of four regimes of device geometry: (d) the 'empty' square billiard, (e) the square with a partially depleted central region, (f) a Sinai billiard formed by the circle at the center of the square billiard, (g) a Sinai billiard featuring a larger circle.

Figure 3 shows the device design used to construct the semiconductor Sinai billiard in our collaboration with the National Research Council in 1995.[24] The major

technological challenge concerned establishing electrical contact to the 0.3μm diameter 'inner' circular gate shown in Fig. 3(b). This was achieved using a bridging interconnect technology developed by one of us (RPT) in the early 1990s.[25, 26] Shown schematically in Fig. 3(c), the fabrication details of this technique are described in detail elsewhere.[1, 25, 26] The proposed device operation was as shown in Fig. 3(d-g): by applying a negative bias V_O to the three 'outer' gates to form a micron-sized square billiard, the circle would then be introduced and enlarged by applying an increasingly negative bias V_I to the inner gate. Because the host material's ℓ value of 25μm was significantly larger than the billiard size, the trajectories of electrons traversing the billiard were expected to be ballistic and to be profoundly affected by this change in geometry. Furthermore, as required by Sinai's model, these electrons would scatter off the walls specularly and elastically.[1, 7] Thus the evolution in billiard geometry shown in Fig. 3(d-g) was expected to be accompanied by Sinai's transition from stable to chaotic dynamics outlined in Fig. 2(a,b).

The proposed experiment would not, however, be the first study of a physical system in which chaotic particles could be tuned. Indeed, transitions had already been achieved in relatively basic systems. For example, chaos had been introduced into the flow of water droplets by adjusting the aperture of a faucet.[27] However, the proposed 'chaotic transistor'[28] offered a number of significant advantages over the dripping faucet as follows. (i) The precision associated with tuning the electrostatic gates was superior to adjustments of the faucet aperture. (ii) The chaos would be introduced into a flow of electrons, raising the possibility of novel electronic applications. For commercial transistors, electrostatic surface gates serve as a switch to modulate the flow of electrons through the device. For the Sinai billiard, the proposed gating operation was considerably more refined - tuning the voltage applied to the gates would induce a controlled evolution in the scattering dynamics of the electrons. By introducing chaos and the associated sensitivity of the trajectories, small controlled changes to the device could lead to large changes in output, leading to efficient switching operations.[28] (iii) In contrast to the classical water droplets, it would be possible to harness the electrons' wave properties and study the device's quantum operation as chaos was 'switched on'.[29]

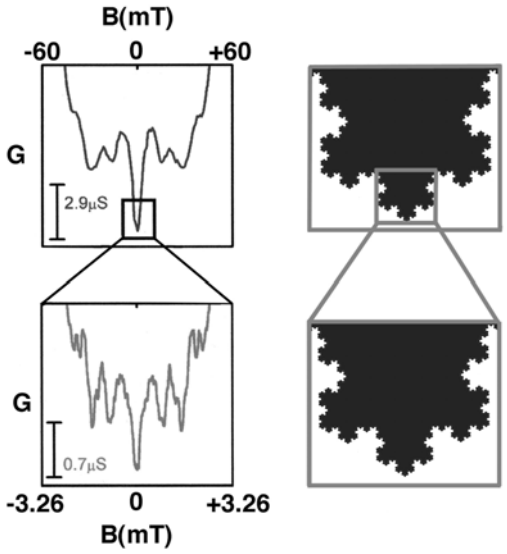

Figure 4 Left: course (top) and fine (bottom) structure observed in the magneto-conductance $G(B)$ measured for $n = 7$. See text for details. Right: the repeating patterns of the Koch Snowflake.

3. The Experimental Observation of Exact Self-Affinity

Directed by these specific aims, initial experiments focussed on the Sinai geometry. Characterisation studies showed that the presence of the central gate could be minimised by setting the bias V_I to +0.7V. A circular depletion region could be formed under the gate by reducing the bias to 0V and for negative V_I the radius R of this depletion circle increased according to the expression $R = R_g - (8 \times 10^{-8})V_I$ (where R_g is the circle's lithographic radius).[28] With the circle activated, we observed that the magneto-conductance fluctuations clustered around two distinct magnetic field scales: 'fine' (f) fluctuations superimposed on 'coarse' (c) fluctuations.[24, 29, 30] This is shown in Fig. 4(left), where V_o has been tuned to set the number of conducting modes, n, in the entrance and exit openings to be 7 and V_I had been tuned to give $R = 0.37\mu m$. This figure was generated by first measuring the c fluctuations (top) using a magnetic field resolution of 1mT and then concentrating on a narrower magnetic field range and adopting a finer resolution of 0.008mT to measure the f fluctuations (bottom). For each level, $G(B)$ was measured for both magnetic field directions (signified in the figure by a change in the sign of B) in order to distinguish between the measurement signal and

measurement noise - due to the Onsager relationships,[7] the signal was symmetric about B = 0T and thus the observed minor deviations from symmetry originated from noise.

We were able to suppress both the c and f fluctuations by increasing V_o to a value sufficiently high to pinch off the channel around the circle, indicating that both sets of fluctuations were generated by circulating trajectories.[24, 30] Furthermore, we were also able to suppress both sets of fluctuations by raising the electron temperature from 50mK (the temperature used in the measurements in Fig. 4(left)) to 4K to remove electron phase coherence,[24, 30] indicating that both sets of fluctuations were generated by wave interference associated with these circulating trajectories. However, their shared qualities extended even further - the patterns observed in the c and f fluctuations appeared to be remarkably similar. To dismiss the possibility that this similarity was simply coincidence, we varied billiard parameters (such as using V_o to adjust n) to induce a change in the c fluctuations and found that the f fluctuations evolved in a similar fashion.[30] This similarity was investigated across an array of fifty bias settings.[31] The observed repetition of patterns observed on different scales clearly bears a close resemblance to mathematical patterns such as the Koch Snowflake shown in Fig. 4(right).[17, 18] To distinguish this exact repetition of the pattern from patterns that merely follow the same statistics at different scales (see later), we labelled the observed behavior as 'exact' self-affinity (ESA).

We confirmed the presence of ESA using a mathematical comparison of the fine scale conductance fluctuations, $\delta G_f(B)$, and the course scale conductance fluctuations, $\delta G_c(B)$. To extract $\delta G_c(B)$ from the c scale conductance trace, $G_c(B)$, we used the definition $\delta G_c(B) = G_c(B) - G_c(B=0)$, and also applied the equivalent definition for $\delta G_f(B)$. For the observed patterns to exhibit ESA, the $\delta G_f(B)$ trace should be a scaled version of the $\delta G_c(B)$ trace and therefore it should be possible to select conductance and field scaling factors, λ_G and λ_B, such that $\delta G_c(B)$ and $\lambda_G \delta G_f(\lambda_B B)$ are nominally identical traces. To quantify this ESA, we introduced a correlation function F:[32]

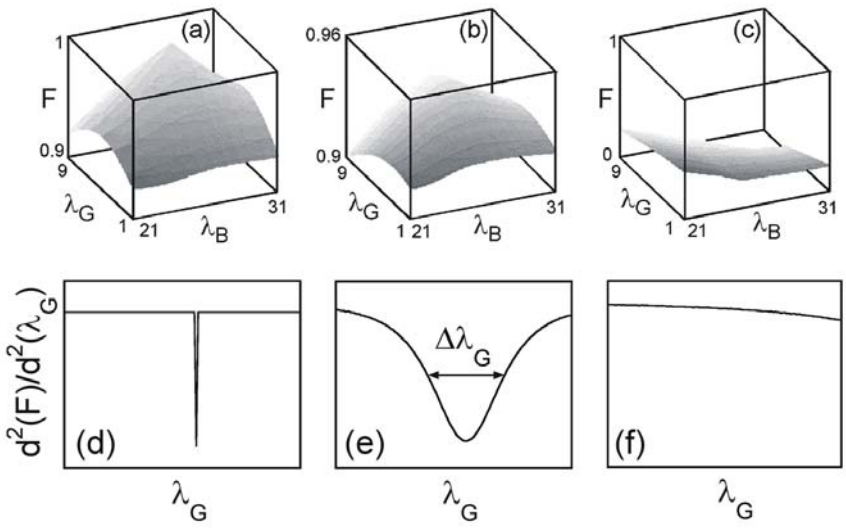

Figure 5 (a), (b) and (c) are scale factor maps, F versus (λ_G, λ_B) for V_o = –0.55V. (a) Circle activated, ideal case; (b) circle activated, experimental case; (c) circle de-activated, experimental case. (d, e, f) are second derivatives of F versus λ_G. V_o = -0.52V.

$$F = 1 - \frac{\sqrt{\left\langle \left\{ \delta G_c(B) - \lambda_G \delta G_f(\lambda_B B) \right\}^2 \right\rangle}}{N} \qquad (1)$$

The averaging <> was performed over 100 magnetic field points between ±50mT. N was introduced as a normalisation constant calculated by averaging 1000 values of the expression $\sqrt{\left\langle \{X(B) - Y(B)\}^2 \right\rangle}$, where $X(B)$ and $Y(B)$ were functions that generated random number distributions over the 100 magnetic field points.[32] Because $\delta G_c(B)$ and $\delta G_f(B)$ were symmetric about B = 0T, $X(B)$ and $Y(B)$ were therefore reflected about B = 0T to ensure the same basic symmetry as the data. The amplitude ranges of $X(B)$ and $Y(B)$ were equated to that of $\delta G_c(B)$. The role of N was to set F = 0 when $\delta G_c(B)$ and $\lambda_G \delta G_f(\lambda_B B)$ were randomly related traces and F = 1 if the two traces were mathematically identical. In this way, F could be used to identify similarities in patterns observed at the two different field scales. Fig. 5(b) is a 'scale factor map', showing F as a function of λ_G and λ_B for the case of R = 0.37μm. A clear maximum of F = 0.94 occurs at λ_G = 6.1 and λ_B = 26.4. Indeed, all scale factor maps obtained for the Sinai billiard (measured for different n values etc) reveal a single peak characterised by F as

high as 0.97.[33] These maps are characteristic of ESA, indicating a striking similarity between the c and f fluctuations. Note, however, that this experimentally-observed ESA is not mathematically perfect. Figure 5(a) is a scale factor map calculated for the ideal case of ESA, where the f fluctuations are a mathematically-generated replica of the c fluctuations. The peak rises to a maximum of $F = 1$ at a singular point in the (λ_G, λ_B) map. This singularity is demonstrated in Fig. 5(d), where the second derivative of F features a δ function at the peak's maximum. Compare this ideal ESA behavior to the experimentally-observed ESA shown in Fig. 5(b): although centerd around the same (λ_G, λ_B) point, the experiment's F peak has a slightly lower value and, as indicated in Fig. 5(e), the peak is less sharp. Ideal ESA was not achieved in the experiment due to contributions from a narrow range of scaling factors rather from a unique pair, and the full widths at half maximum extracted from the second derivative plots quantified this range as $(\Delta\lambda_G, \Delta\lambda_B) = (2.7, 1)$.[33] We will return to this observation in the next section.

Having established that the two sets of fluctuations (c and f) exhibited ESA, the next step was to determine if they were also fractal. To be fractal, the fluctuations should not be limited to two magnetic field scales but instead should continue to cluster at increasingly fine and increasingly course scales, building up a cascade of levels spanning many field scales. Furthermore, as with the Koch Snowflake, there should be a constant magnification factor separating neighbouring levels. For our fluctuations, this would be set by the magnetic field scale factor λ_B. For the data of Fig. 4(left), λ_B was found to have a value of 18.6. Therefore, for the magneto-conductance to be fractal, we should be able to 'zoom' into the f level by a magnification factor of *precisely* 18.6 and observe an additional cluster of fluctuations. This was found to be the case and we labelled this as the ultra-fine (uf) level.[29, 32] Similarly, we zoomed out from the c level by precisely 18.6 and found the ultra-course (uc) level.[34, 35] A full discussion of the ESA analysis and visual inspections of the uf and uc fluctuations can be found elsewhere.[35] Significantly, we found that, in addition to the common field scaling factor λ_B, the four levels of fluctuations (uf, f, c, uc) were described by a common conductance scaling factor λ_G, as required for fractal patterns.[12, 17, 18] The final step for establishing fractal behavior involves an examination of the relationship between the two constant scaling factors, λ_B

and λ_G. These factors relate to a crucial parameter for characterising fractal patterns called the fractal dimension *D*. Whereas *F* quantifies the similarity between the patterns observed at different magnifications, *D* quantifies their scaling relationship.[17, 18] For Euclidean patterns, dimension assumes the familiar integer values: for a smooth line, *D* has a value of 1, whilst for a completely filled area its value is 2. However, for a fractal pattern, the repeating structure at different magnifications causes the line to begin to occupy area. *D* then has a fractional value between 1 and 2 and, as the complexity of the repeating structure increases, its value moves closer to 2. To confirm that the four levels observed in *G*(*B*) were fractal it was therefore necessary to show that their scaling relationship was described by a fractional value of *D*.

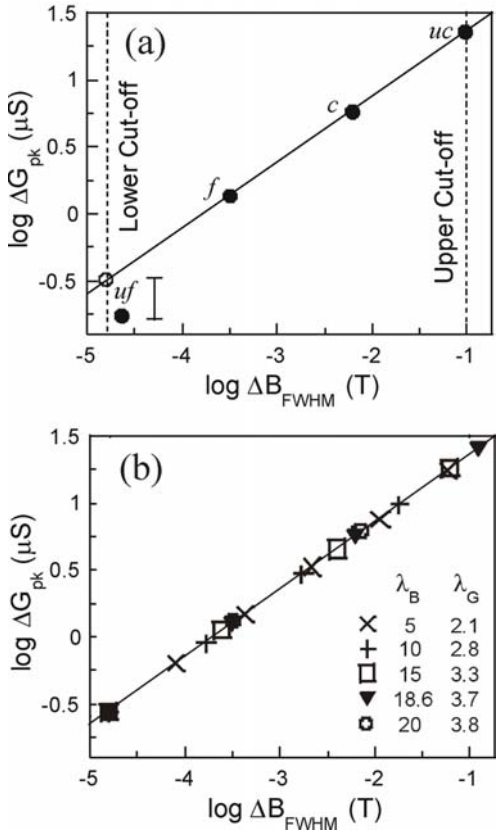

Figure 6 (a) Scaling properties of the levels observed in the experimental data based on the central peak height ΔG_{pk} and full width at half maximum ΔB_{FWHM}. The four points (*uf*, *f*, *c* and *uc*) represent a single hierarchy described by $\lambda_B = 18.6$. (b) A scaling plot showing four additional λ_B values and their associated hierarchies.

To calculate *D* from the scaling relationship of the four observed levels, we constructed scaling plots such as the one shown in Fig. 6(a). For simplicity, here we show the analysis performed on one selected feature within each cluster of fluctuations –

the peak in resistance observed around B = 0T. We quantified the peak's scaling properties using ΔB_{FWHM} (the full width at half maximum) and ΔG_{pk} (the peak's height) and obtained the four filled circles shown in Fig. 6(a).[32, 35] With the exception of the *uf* data point (discussed below), the data condenses onto the power law line shown. Note that, as expected, the four levels lie at equal increments along the power law line, indicating that the conductance amplitudes and magnetic field periods of consecutive levels can be related by the common field and conductance scaling factors $\lambda_B = \Delta B_m/\Delta B_{m+1}$ and $\lambda_G = \Delta G_m/\Delta G_{m+1}$ respectively (here the indices m = 1 - 4 have been assigned in order of decreasing scale - i.e. the *uc* level corresponds to m = 1 and *uf* to m = 4). Furthermore, these scaling factors are related by the power law relationship $\lambda_G = (\lambda_B)^{\beta}$. Such a scaling behavior is defined as fractal if the fractal dimension $D = 2 - \beta$ lies in the range $1 < D < 2$.[12] Allowing for uncertainties in the *uf* point (see below), the data points in Fig. 6(a) all lie on a line whose gradient β gives D = 1.55, confirming that the four observed clusters of fluctuations are fractal.

The dashed vertical lines in Fig. 6(a) provide the experimental observation limits of this fractal behavior and we label these the upper and lower 'cut-offs'. The lower cut-off was determined by the magnetic field resolution limit for the experiment. Although the separation between measured magnetic field points was 0.008mT, a minimum of three data points was required to observe a feature in $G(B)$. Thus the lower cut-off for the experiment corresponds to an interval ΔB of 0.016mT and this magnetic field value is indicated by the left dashed line. Note that the *uf* fluctuations lie on this resolution limit. The *uf* trace consists of only 46 data points compared to the 788 data points within the equivalent *f* trace and the distortion caused by the limited resolution of *uf* has been used to account for the slight difference in ΔB_{FWHM} (0.004mT) between the *uf* point's actual position (filled circle) and its anticipated position on the power law line (open circle).[35] As indicated by the 2Ω adjacent bar, the difference in ΔG_{pk} between the measured and anticipated position of the *uf* point lies within the noise limit of the experiment (0.05% of the signal, corresponding to ~3Ω). As a consequence of these

measurement limitations, it was not possible to observe further levels of clustered fluctuations at finer field scales beyond the *uf* level.

At the other end of the scaling plot, the calculation of the position of the upper cut-off was based on the magnetic field at which the cyclotron radius of the electron becomes smaller than the billiard size. Above this field limit a transition to electron transport via skipping orbits occurs and the Sinai diffuser is no longer expected to induce chaos in the trajectories in the manner shown in Fig. 2(b). Accordingly, in the experiment the magnetic field traces were only measured up to this B field, and this sets the maximum possible ΔB value. Note that the *uc* trace lies at the upper cut-off limit. As expected, further levels of clustered fluctuations at field scales larger than the *uc* level were not observed. The range of observation of fractal behavior defined by the upper and lower cut-offs shown in Fig. 6(a) is 3.7 orders of magnitude in ΔB.[34] This scaling range is well in excess of the majority of observations of fractals in other physical systems - a recent survey revealed a typical range of less than 1.5 orders.[36] This extended range of observation makes the Sinai billiard an ideal system in which to investigate the scaling relationships of fractal phenomena.

4. The Interpretation of Exact Self-Affinity

The primary aim of the 'chaotic transistor' experiment was to induce chaos in the classical trajectories by activating the Sinai diffuser, and then to investigate how the classical chaos affected the conductance in the quantum regime. However, although the classical trajectories were expected to follow the transition outlined in Fig. 2(a,b), there were crucial differences between Sinai's original concept and the experiment. Firstly, whereas the theoretical Sinai billiard of Fig. 2 was 'closed', the semiconductor Sinai billiard of Fig. 3 incorporated openings in the walls to inject the electrons and thus facilitate current flow. This is a significant difference because current injection processes typically play a major role in determining the conduction properties of ballistic devices.[37] Secondly, Sinai's model was purely classical and offered no prediction for how the chaos would translate in the quantum regime. Consequently, at the time of the experiment,

there was considerable debate over the precise form in which the quantum chaos would emerge in the measurements. One possibility was that the Sinai billiard would reveal similar magneto-conductance characteristics to the chaotic stadium investigated in the original studies of quantum chaos.[8] In this original experiment, the amplitude of the fluctuations had been shown to have an exponential dependence on the period ΔB. Applying a semi-classical model based on the Aharonov-Bohm concept discussed earlier, this dependence was interpreted as being a consequence of an exponential distribution of classical trajectory loops within the billiard. This result was appealing because an exponential distribution of loop areas was thought to be a universal signature of chaotic billiards.[38] However, the Sinai billiard's fractal dependence of fluctuation amplitude on ΔB stood in sharp contrast to the stadium's 'universal' signature of chaos. Why, then, was the Sinai billiard - the model system for demonstrating chaos - producing fractal properties in the conductance fluctuations?

A plausible explanation emerged soon after the experiments were completed. The 2DEG of the semiconductor Sinai billiard was located 163nm below the surface gates and, as a consequence, our simulations showed that the electrostatic walls differed from Sinai's model in a crucial respect. Whereas Sinai's model billiard was described by so-called 'hard' walls with vertical energy profiles, the depletion regions penetrating the 2DEG defined a billiard with electrostatic walls featuring approximately parabolic energy profiles.[39] Figure 2(d) shows the 'soft' wall profile for the semiconductor Sinai billiard of Fig. 3(a,b). A comparison of Figs. 2 and 3 reveals the striking difference between the straight shapes of the surface gate pattern and the smoother, rounded shapes of the billiard walls that form in the 2DEG. Such simulations signalled that modelling of semiconductor ballistic transport was destined to be more subtle than initially anticipated. Mapping of the ballistic trajectories would require more than knowledge of the surface gate pattern - details of the wall's precise energy profile at the 2DEG would also be necessary. Although this revelation emphasised an intrinsic limitation of semiconductor billiards, a positive side to this discovery quickly emerged - the trajectories predicted for 'realistic' soft-walled billiards displayed remarkably intricate and exotic properties compared to those predicted for their 'ideal' hard-walled counterparts! In particular, soft-wall billiards were predicted to generate 'mixed' electron dynamics featuring *both*

stable and chaotic trajectories.[16, 39, 40] Significantly, mixed systems are well-known for generating complex behavior such as fractals at the borders between stability and chaos.

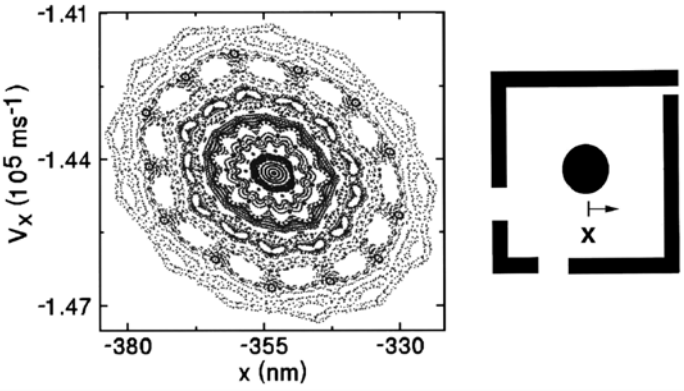

Figure 7 A Poincaré section for the Sinai billiard, showing that structure in the position (x) versus velocity (v_x) phase space plot occurs at many magnifications. The x position is indicated in the schematic diagram of the billiard.

Our first approach to establishing a link between the mixed trajectory dynamics and the measured ESA was to model the *precise* soft-wall profile of the semiconductor Sinai billiard - including perturbations from impurities, defects and surface states.[39] To detect any underlying order in the classical trajectories generated from this realistic model of the potential profile, we then mapped out the velocities and positions of the electrons.[39] A typical Poincaré plot is shown in Fig. 7 and, significantly, reveals structure occurring at many magnifications. This raises the possibility that the fractal character of the conductance fluctuations is essentially classical in origin and that the role of the quantum wave interference is to serve as a conduction process that is sensitive to this repetition of the classical structure. Due to the remarkably rich character of the structure, determination of the individual trajectories that generate the observed ESA has proven difficult. In response, we adopted a parallel approach to the understanding of the ESA that treated the conductance fluctuations as a 'fingerprint' of the contributing trajectories. By fitting the fluctuations, we were able to identify a possible set of trajectories that generate the precise experimental features of the ESA.[41] These trajectories form loops similar to those predicted for the hard-wall Sinai billiard.[42] The effect of the soft-wall profile of the measured semiconductor billiard appears to be to modify the coefficients that determine the relative contributions of these loops to the conductance. We found that if we modified these coefficients so that they followed a Weierstrass scaling

relationship (a function well-known in mathematics for generating ESA)[12, 43] then the experimentally observed fluctuations could be reproduced with remarkable accuracy.[41] However, what remains unclear is precisely how the realistic soft-wall profiles produce this modification.

Whereas a detailed explanation for the origin of the observed ESA proved to be elusive, the experiment served to demonstrate the differences between ideal and realistic semiconductor billiards. Following the experiment, both the Sinai geometry and the 'empty' square geometry were pictured as mixed trajectory systems rather than the purely stable and purely chaotic systems predicted for the two equivalent hard-wall geometries of Fig. 2(a,b). Whereas insertion of the central circle had originally been modelled in terms of a Sinai diffuser converting stable to chaotic trajectories, this gating operation was now pictured as a 'plunger' gate, fine-tuning the relative contributions of the stable and chaotic trajectories within the mixed trajectory system. In particular, the plunger was viewed as a trajectory 'selector.' Within this picture, on activation of the plunger, large parts of the Poincaré plot would become exclusion regions and all but a selected set of trajectories would be removed from the billiard system. De-activation would re-introduce the forbidden trajectories, producing Poincaré plots of increased complexity. Consequently, the transition from Sinai billiard to empty square was predicted to be accompanied by a sharp increase in complexity in the observed conductance fluctuations.

This model of trajectory selection was developed further in terms of an associated selection of the scaling factors (λ_B, λ_G). Whereas a full mathematical framework is presented elsewhere,[33, 44] here we summarise the essential results using the scaling plots shown in Fig. 6. As discussed earlier, the ESA observed for the Sinai billiard was generated by a single hierarchy of points (m = 1, 2, 3, 4....) located along the line with gradient $\beta = 2 - D$. The four points each satisfy the power law relationship $\lambda_G = (\lambda_B)^{\beta}$ and are separated by equal spacings along the line determined by λ_B = 18.6. According to the model, as the circle's size is reduced, introduction of extra trajectories leads to an increase in the number of allowed values of λ_B. For each allowed λ_B value there exists a hierarchy of points (m = 1, 2, 3, 4....) lying on the same power-law line with

a spacing set by the λ_B value. For simplicity, in Fig. 6(b) we have shown just four additional λ_B values and the associated hierarchies. As the circle is reduced further, and the number of allowed λ_B values increases, the power law line gradually becomes filled with points at all ΔB values. This is expected to have a striking impact on the appearance of the conductance fluctuations. Firstly, since each data point represents a cluster of fluctuations observed at a particular ΔB magnification (see Fig. 4), then fluctuations should be observed at *all* magnifications for the empty square. Secondly, fluctuations belonging to different hierarchies coincide at the same ΔB magnification causing them to merge and lose the exact repetition characteristic of ESA. This predicted behavior is confirmed in the magneto-conductance fluctuations shown in Fig. 8(left) measured for the square billiard geometry. The observed fluctuations are strikingly different from those of the Sinai billiard shown in Fig. 4(left). As predicted, the fluctuations no longer cluster around selected magnetic field scales but instead are evident at *all* ΔB scales. Secondly, regardless of the magnification factor chosen, the patterns observed at different scales are clearly different: ESA is no longer observed.

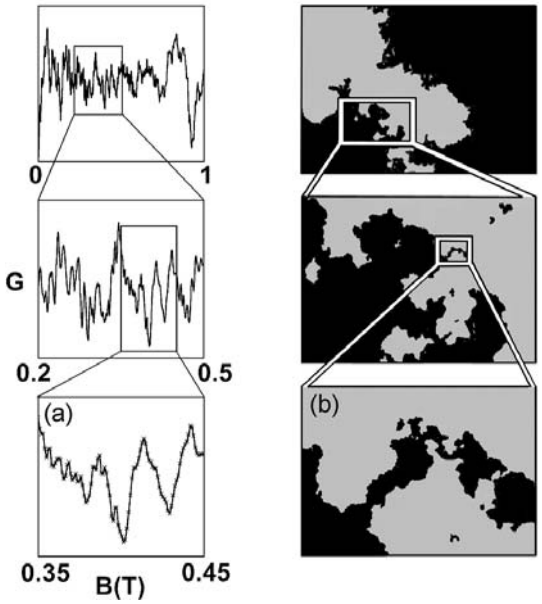

Figure 8 (a) Statistical self-affinity for an empty billiard. Similar to the coastline shown in (b), $G(B)$ does not reveal an exact repetition of patterns at different magnifications.

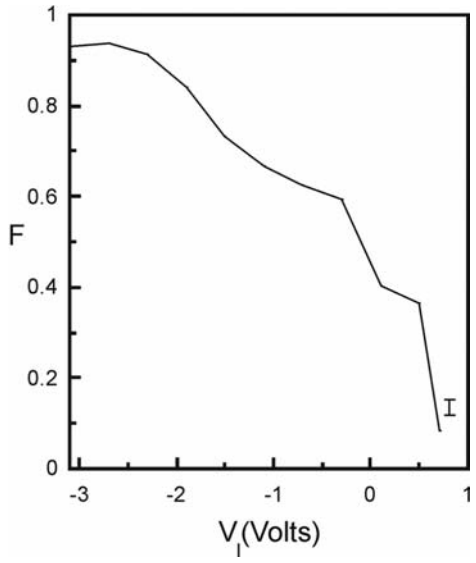

Figure 9 The transition from the Sinai billiard to the empty square billiard, charted by F versus V_I. The trace is taken for $n = 7$.

In Fig. 9 we have used the correlation analysis to examine the suppression of ESA during the transition from the Sinai billiard to the 'empty' square billiard.* As noted earlier, for the largest circle radius investigated in the experiment ($R = 0.37\mu m$), a narrow range of scaling factors was already present rather than the unique pair required for ideal ESA. It appears, therefore, that at $R = 0.37\mu m$ the circle was not quite large enough to act as a 'perfect' scale factor selector. The full widths at half maximum extracted from the second derivative plots of Fig. 5(e) quantified this range in scale factors as $(\Delta\lambda_G, \Delta\lambda_B) = (2.7, 1)$. This range produced the small degradation in ESA from the ideal case of $F = 1$ to the observed value of $F = 0.94$ for $R = 0.37\mu m$. In Fig. 9, $R = 0.37\mu m$ corresponds to the bias $V_I = -3.1V$. Moving from left to right, Fig. 9 shows that an increase in V_I towards 0V was accompanied by a rapid fall in F, indicating a dramatic loss in ESA as the circle size was reduced and the range of allowed scale factors was increased. For $V_I = +0.7V$ (corresponding to the minimised presence of the circle) the correlation has fallen to less than $F = 0.1$. The scale factor map for the empty billiard is shown in Fig. 5(c,f) and this fails to yield the well-defined single maximum found in the

---

* The error bar in Fig. 9 represents the difference between the F value obtained by correlating two nominally-identical $\delta G_c(B)$ traces taken in opposite magnetic field directions and the expected value of $F = 1$. Therefore any deviations in F greater than this indicator can be regarded as significant.

equivalent plot of Fig. 5(b,e) for the Sinai billiard. Instead, the plot reveals a smooth contour with an average value of F well below 0.2 for all values of (λ_G, λ_B).* This scale factor map is a signature of a $G(B)$ trace that no longer contains an exact repetition of patterns at different field scales.

5. The Observation of Statistical Self-Affinity

In the last section, we saw that the model of the central circle as a trajectory selector, developed during 1996-7, successfully describes the suppression of ESA observed in the conductance fluctuations during the transition from the Sinai billiard to the empty square billiard. The model also offers further crucial predictions for the transition. Because all the hierarchies shown in the scaling plot of Fig. 6(b) lie on the same power-law line, the scaling properties of all the fluctuations are described by a common D value.[32, 33, 44] Therefore, according to the model, fractal behavior should be preserved during the transition. This can be demonstrated mathematically as follows.[33] Starting with the analysis of Fig. 6(a), we saw that the fractal scaling behavior of ESA is described by $\lambda_G = (\lambda_B)^{\beta}$, where $\lambda_B = \Delta B_m/\Delta B_{m+1}$ and $\lambda_G = \Delta G_m/\Delta G_{m+1}$ respectively. If we perform an equivalent analysis replacing ΔG_m (the conductance amplitude of a selected feature in the mth cluster) with $< \{\delta G(B) - \delta G(B + \Delta B_m)\}^2 >$ (the variance of $\delta G(B)$ with ΔB_m for the mth cluster), we obtain an analogous ESA power law expression:

$$\frac{< \{\delta G(B) - \delta G(B + \Delta B_m)\}^2 >}{< \{\delta G(B) - \delta G(B + \Delta B_{m+1})\}^2 >} = \left(\frac{\Delta B_m}{\Delta B_{m+1}} \right)^{\gamma} \quad \text{where} \quad \lambda_B = \left(\frac{\Delta B_m}{\Delta B_{m+1}} \right) \qquad (2)$$

and $D = 2 - \gamma/2$. Note that this equation, representing the scaling behavior shown in Fig. 6(a), has a unique λ_B value and holds only for ΔB values corresponding to the cluster field scales ΔB_m. In contrast, for the scaling behavior represented in Fig. 6(b), this condition is relaxed: the system has a continuous range of λ_B values and, consequently, the power law

---

* As for all plots, the observed background has a slope set by the condition (λ_G, λ_B, F) = (1,1,1). For more details see reference 33.

holds for all values of ΔB. The power law expression describing Fig. 6(b) therefore has the form:

$$< \{\delta G(B) - \delta G(B + \Delta B)\}^2 > \propto (\Delta B)^{\gamma} \qquad (3)$$

where $D = 2 - \gamma / 2$. Significantly, this form of equation is well-known within fractal studies. Commonly referred to as 'fractional Brownian statistics,' this scaling relationship has been used to describe a diverse range of natural fractal phenomena.[17, 45] As shown in the coastline picture of Fig. 8(right), fractals observed in nature don't exhibit ESA.[17, 18] Rather than an exact repetition, the coastline patterns observed on different scales simply follow the same statistical relationship - 'statistical self-affinity' (SSA).

The relatively simple mathematical steps outlined above therefore predict that the evolution from the Sinai to square geometry should be accompanied by a transition from ESA to SSA in the magneto-conductance fluctuations. If this prediction turned out to be correct then soft-walled semiconductor billiards would represent a truly remarkable environment for the study of fractal behavior - transitions between the two forms of fractals (ESA and SSA) had never been observed in a physical system. Furthermore, this possibility of observing SSA was particularly intriguing because, a year earlier, an independent theoretical investigation had also predicted SSA for soft-walled semiconductor billiards.[16] This elegant theory proposed that structure at the boundaries between chaotic and stable regions of the mixed trajectory system might be described in terms of an infinite hierarchy of Cantori[12, 17, 19] and that the Cantori would strongly influence the wave chaos properties of the soft-wall billiards.[16] The presence of Cantori was predicted to produce a power-law distribution of classical loop areas and, through a semi-classical wave interference process, this would be detected as fractal scaling of the conductance fluctuations.[16] Specifically, the relationship between the measured D and the power law exponent γ was predicted to be $D = 2 - (\gamma / 2)$.

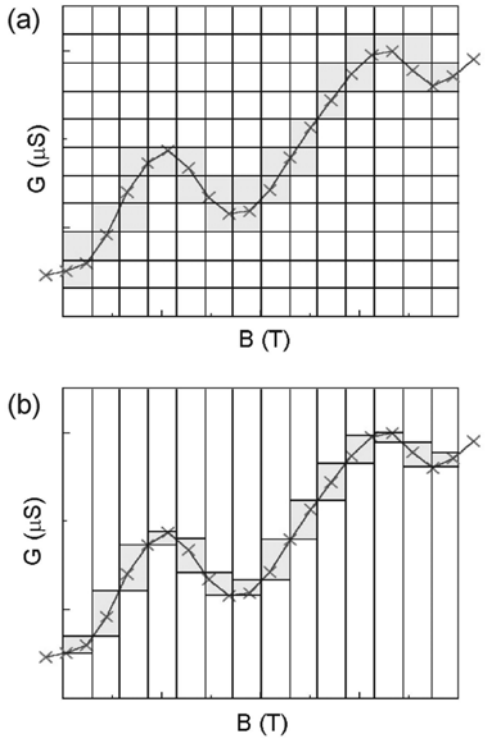

Figure 10 Schematic representations of (a) the box counting technique and (b) the Variation method.

To confirm that the fractal character of the magneto-conductance fluctuations had indeed been preserved during the Sinai to square transition, we had to demonstrate that the scaling relationship of the fluctuations could still be described by a fractional value of *D*. For the ESA observed in the Sinai billiard, the *D* value was calculated by identifying specific features in the fluctuations and then plotting their sizes at different magnifications (see Fig. 6(a)). However, because there was no longer an exact repetition of features, this approach was not possible for SSA. Rather, it was necessary to calculate how the statistical qualities of the fluctuation patterns scaled. To do this, we employed four well-established methods for fractal detection and found them to be consistent.[46] One approach, based on Equation (3), is to obtain a linear fit to the plot of $\log[< \{\delta G(B) - \delta G(B + \Delta B)\}^2 >]$ versus $\log(\Delta B)$. However, here we will concentrate on a more traditional method of fractal analysis known as the 'box-counting' technique.[17, 18, 46] A comparison of the relative advantages of the two techniques can be found elsewhere.[46] The box-counting technique is shown in the schematic representation of Fig. 10(a). The magneto-conductance trace is covered with a computer-generated mesh of identical

squares (or 'boxes'). The statistical qualities of the fluctuation patterns can then be determined by analysing which squares are occupied by the trace (shaded in Fig.10(a)) and which are empty. These statistics can then be compared at different magnifications by reducing the square size in the mesh. In particular, D can be obtained by calculating the number of occupied squares in the mesh, $N(\Delta B)$, as a function of square size ΔB. For fractal behavior, $N(\Delta B)$ scales according to $N(\Delta B) \sim \Delta B^{-D}$ where $1 < D < 2$.[17, 18] Therefore, by constructing a scaling plot of $-\log N(\Delta B)$ against $\log \Delta B$, the fractal behavior is detected as a straight line and quantified by extracting D from the gradient. This scaling plot, shown in Fig. 11, is equivalent to the one shown in Fig. 6(a) that we used for the case of ESA.*

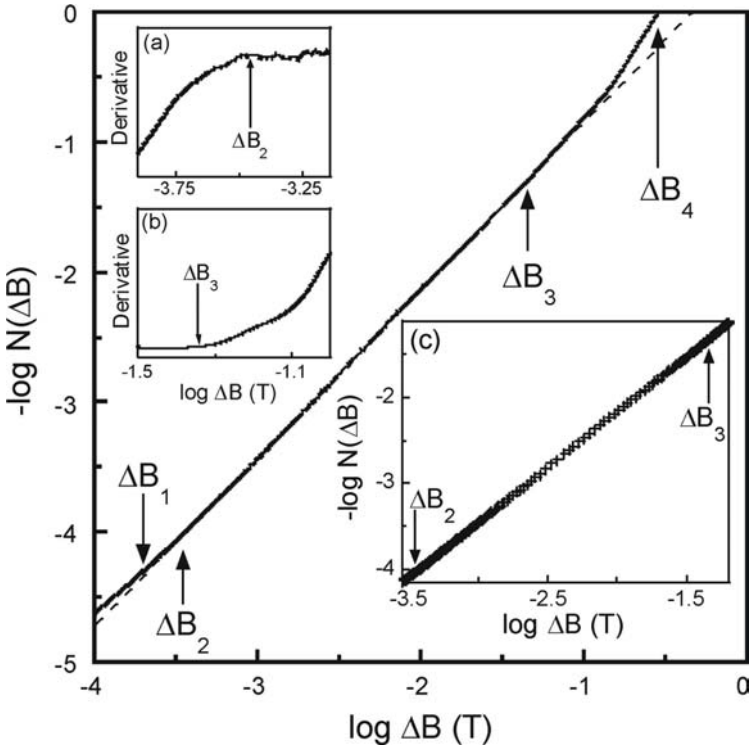

Figure 11 The scaling plot for an empty billiard. The data (solid) follows a straight line (dashed line) between the magnetic field scales ΔB_2 and ΔB_3. Insets (a) and (b) are derivative plots of the data and (c) shows the individual data points (for clarity only every tenth point is shown).

---

* Note that the exponent of the power law relationship used in Fig. 6(a) is 2 - D whilst the exponent used in Fig. 11 is -D. The reason for this difference is as follows. D is a 'covering' dimension – it measures the amount of area covered by the trace at different magnifications (see references 17,18). To convert the box count N into a covered area, N should be multiplied by the box area $(\Delta B)^2$. This then converts the $-D$ exponent used in Fig. 11 into the 2 - D exponent used in Fig. 6(a).

In 1997 we published results reporting that the square billiard geometry generates SSA.[47] As predicted, fractal behavior was preserved during the transition from the Sinai billiard to the empty square. The transition from R = 0.37μm to (nominally) R = 0μm was accompanied by a smooth reduction in D by approximately 10%. We note that, although the presence of the circle was minimised at V_I = +0.7V, we cannot exclude the possibility that remnants of the circle remained. Therefore, to confirm that this second form of fractal behavior, SSA, does not require the presence of a circle, we constructed a billiard with an identical geometry to the one shown in Fig. 3 but without the central circular gate. Fig. 11 shows a typical scaling plot obtained for this billiard (T = 50mK and n = 6) and this confirms that the completely empty billiard generates SSA. The dashed straight line is a guide to the eye, indicating that the data follow the fractal scaling relationship between the magnetic field scales ΔB_2 and ΔB_3. The values of these upper and lower cut-offs are determined using the derivative plots shown in Fig. 11 (a,b). The field scale marked ΔB_1 represents the magnetic field resolution limit. However, the data remain non-fractal up to ΔB_2 due to the dominance of measurement noise over signal for these small fluctuations in *G(B)*. Note, therefore, that for both ESA (Fig. 6(a)) and SSA (Fig. 11), the lower cut-off is set by noise restrictions. Just as with the case of ESA, the upper cut-off for observing SSA is set by the emergence of non-fractal (skipping orbit) conduction processes at higher fields. This change in conduction processes is marked as B_{cyc} in Fig. 12. This limits the length of the data trace to B < 150mT and this is marked

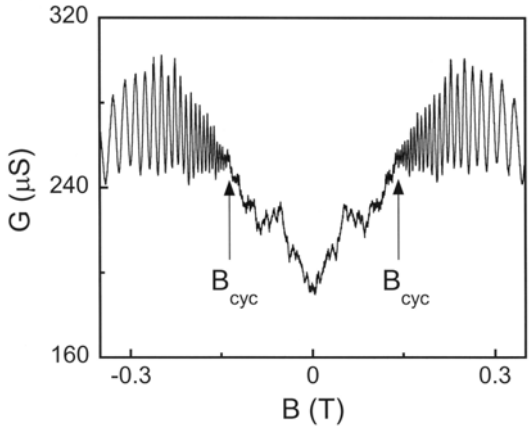

Figure 12 A plot of $G(B)$ showing the change in conductance behavior above the magnetic field B_{cyc} at which the cyclotron radius fits within the billiard size. Above this field, electron transport is described by skipping orbits and the conductance is non-fractal. B_{cyc} therefore forms the ΔB_4 cut-off shown in Fig. 11.

as ΔB_4 in Fig. 11. The upper cut-off in fact occurs at the field scale marked ΔB_3, which is slightly below ΔB_4. The field scale ΔB_3 forms the upper cut-off rather than ΔB_4 because it is necessary to fit at least 50 squares in the mesh in order to achieve sufficient box-counting statistics to resolve the fractal behavior.[17, 18, 46]

Fig. 11(c) focuses on the data lying within the fractal scaling regime and shows the individual data points. To produce this plot we employed two refinements to the box-counting method – the Variation method (for which the data point density increases at small ΔB) and the Horizontal Structured Elements method (for which the density increases at large ΔB).[48] Here we briefly discuss the Variation method, which is compared to the basic 'box-counting' method in the schematic of Fig.10. Strictly speaking, the technique of extracting D should calculate the minimum number of non-overlapping boxes required to cover the data trace. Although the boxes shown in Fig.10(a) are not overlapping, the rigidity provided by the mesh leads to a small over-estimation of the number of boxes required to cover the data trace. We remove this error using the Variation method, where vertical columns of width ΔB are used rather a mesh of squares of size ΔB. The total shaded area shown in Fig. 10(b) is then calculated and divided by the unit box size $(\Delta B)^2$ to obtain the minimum number of boxes required to cover the trace. By adopting the Variation and Horizontal Structured Elements methods rather than the simple box-counting method we remove errors in the D value, and by combining the two methods on one scaling plot we achieve a high data point density across all ΔB values, ensuring a reliable detection of fractal scaling. The gradient of the dashed line shown in Fig. 11 corresponds to $D = 1.29$.

Whereas we use plots such as Fig. 11 to quantify 'fractal scaling' - the statistical relationship between patterns observed on different magnification scales - we also use plots such as Fig. 13 to investigate 'fractal displacement' - the statistical relationship between patterns observed at different magnetic field locations along the trace. In Fig. 13(d) we show an experimental $G(B)$ trace ($n = 3$) that exhibits SSA with $D = 1.28$. To quantify how the statistical qualities of patterns vary along the $G(B)$ trace, we introduce the concept of a 'local' fractal dimension D_L. Whilst D is the 'universal' fractal

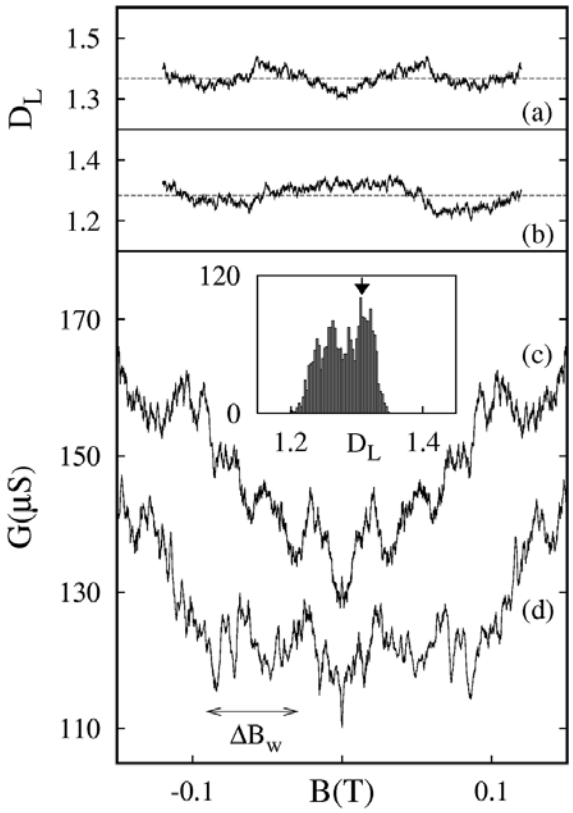

Figure 13 Investigations of fractal displacement. (a) A plot of local fractal dimension D_L versus window position for the simulated $G(B)$ trace shown in (c). The D_L value 'meanders' around the D value indicated by the dashed line. (b) A similar plot for the experimental $G(B)$ trace shown in (d). The histogram plots the distribution of D_L around the D value (indicated by the arrow) for the experimental case.

dimension, extracted from a scaling plot that assesses the full length of the $G(B)$ trace, D_L is extracted from a scaling plot that assesses only a selected region of the trace. The window size of this region is indicated by the horizontal bar next to the experimental $G(B)$ trace (ΔB_w= 60mT). Fig. 13(b) shows the D_L value plotted as a function of the B field location of the window's center along the experimental $G(B)$ trace. The D_L value 'meanders' around the D value of the trace (indicated by the dashed line). We stress that this variation in D_L is not a random variation due to measurement restrictions associated with fitting over a narrow range in the scaling plot (this random variation is significantly smaller and can be seen superimposed on the 'meander' variation). The histogram shows the distribution of D_L values around the D value (indicated by the arrow). Due to the

limited number of points, it is not possible to determine the exact distribution.* We note, however, that a $G(B)$ trace (Fig. 13(c)) generated by fractional Brownian statistics[12, 17, 45] with an identical D value to the experimental trace has a very similar meander (see Fig. 13(a)) to that revealed by the experimental data. This behavior of the local dimension D_L meandering around a constant D value is significant – the fact that D does not evolve with magnetic field indicates that, over the range considered (-150mT< B < 150mT), the changing field is not altering the dynamics of the classical loops. This result is in contrast to other studies, where application of a magnetic field has been pictured in terms of altering the mixed character of the system and enhancing the fractal conductance.[49]

6. The Classical to Quantum Transition: how do Fractals "Disappear?"

Since the initial Sinai experiment in 1995, a number of research groups have observed SSA in soft-walled semiconductor billiards.[49, 50, 51] Whereas most of these studies have varied the electron phase by sweeping magnetic field, others have used a back-gate to vary the phase through a changing Fermi energy E_F.[49] In our own experiments spanning the period from 1995 to 2000, we measured SSA for an unexpectedly wide range of billiard parameter values. Furthermore, SSA has even been observed in gold nano-wires.[52] This prevalence of SSA suggests a remarkably robust phenomenon, prompting us to ask a fundamental question - how do fractals deteriorate into non-fractal behavior as the generating process is gradually suppressed? Whereas this question could, in principle, be applied to any fractal system, the semiconductor billiard is of particular interest for two distinct reasons. Firstly, many studies of fractals are 'passive,' where rather than actively interacting with the process generating the fractals, the experiments are limited to a simple monitoring role.[18] In contrast, the parameters thought to influence the fractal behavior in the billiard system can be adjusted with precision, allowing a systematic study. Secondly, whereas most of nature's fractals are classical in origin,[17] the billiard's fractals were thought to arise from a semi-classical

---

* The only way to increase the number of points plotted in the distribution is to decrease the window size. However, this increases the random variations in D_L due to the narrower fitting range used in the scaling plots.

process (see Sections 1 and 5). We planned therefore to suppress this semi-classical process using controlled transitions towards fully classical and fully quantum-mechanical conduction.

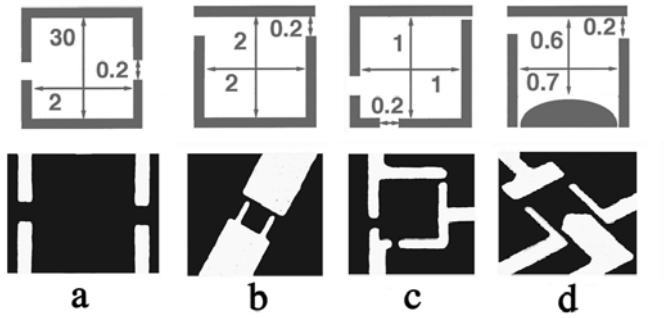

Figure 14 Schematics of the gate patterns (not to scale) together with the equivalent scanning electron micrographs for four (*a*, *b*, *c* and *d*) of the seven billiards used to investigate the classical-quantum transition. The dimensions are in μm. Billiards *e*, *f* and *g* have the same geometry as *b* but are different sizes (see Table 1).

To span the full experimental range of classical, semi-classical and quantum conduction in a comprehensive fashion, in 2000 we re-visited all of the data we had accumulated over the previous five years and also performed new experiments in the parameter ranges previously unexplored.[53] Figure 14 and Table 1 summarize the properties of the seven billiard investigated. Billiards with similar Fermi wavelengths

Device	A (μm^2)	T (K)	ℓ (μm)	n	τ_q(ps)	Q
a	60.0	0.03	25	4	16.6	0.003
b	4.0	0.03	4.4	2	109.6	0.30
c	1.0	0.03 – 4.2	12	2-6	2.8-182.9	0.012 – 1.99
d	0.22 – 0.09	0.03	5.5	2	75.0-87.9	4.34 – 9.05
e	1.0	0.03 – 4.2	4.4	2	24.9-113.2	0.02 – 1.23
f	0.36	0.03 – 2.5	4.4	2	20.1-98.7	0.08 – 2.96
g	0.16	0.03	4.4	2	83.4	5.67

Table 1: a summary of the billiard parameters discussed in Section 6 of the text.

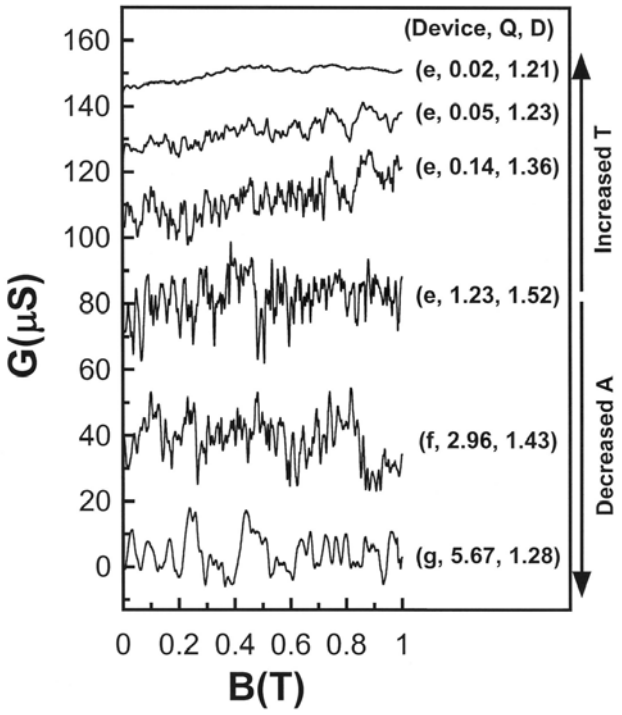

Figure 15 Magneto-conductance fluctuations measured for billiards *e*, *f* and *g* (see trace labels) with $n = 2$ and $\ell = 4.4\mu m$. From top to bottom the (T, A) values for the traces are (4.2K, 1.0μm^2), (1.4K, 1.0μm^2), (0.48K, 1.0μm^2), (0.03K, 1.0μm^2), (0.03K, 0.36μm^2) and (0.03K, 0.16μm^2). The right-hand brackets indicate (Device, Q, D) (see text for the definition of Q). The traces are offset vertically for clarity.

(typically 40 nm) but different sizes (ranging from 0.4μm to 30μm billiard width) were studied at different temperatures (ranging over two orders of magnitude from 0.02 K to 2 K). We started by considering a typical micron-sized billiard (device *e*) where the ratio S of the billiard size to the Fermi wavelength was 22, ensuring semi-classical transport.[10, 11, 16] The magneto-conductance measured at T = 30mK (corresponding to an electron phase coherence length of 30μm) is shown in the fourth (from top) trace of Fig. 15 and reveals the complex fluctuation patterns expected for FCF behavior. The remaining traces in Fig. 15 demonstrate the effect of varying T and the area enclosed by the billiard A. An increase in T reduces the electron phase coherence length and is therefore expected to induce more classical conduction. In contrast, a decrease in A reduces S and should therefore increase the importance of purely quantum-mechanical transport processes. It is clear from Fig. 15 that the complexity of the measured fluctuations decreases by increasing T (moving to the upper traces) or reducing A (moving to the lower traces obtained from the smaller billiards *f* and *g*). This suggests that deviations

from semi-classical conduction within the billiard induce a profound change in the scaling properties of the fluctuations.

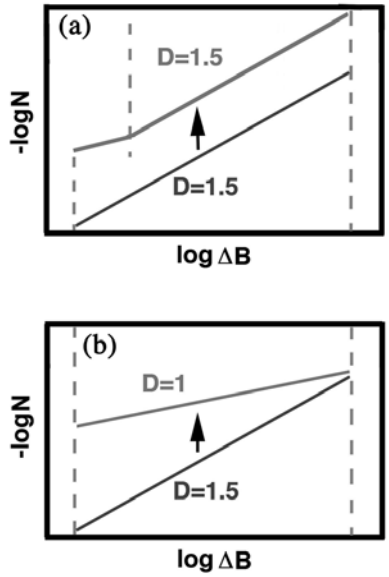

Figure 16 Schematic representations of scaling plots showing (a) the scenario of fractal deterioration anticipated from semi-classical theory, and (b) the measured evolution in fractal behavior.

At first, this observation seemed to be in agreement with theoretical expectations: as a semi-classical phenomenon, the FCF should smooth out in the classical and quantum regimes.[16, 50] To quantify the observed changes in scaling behavior we employed the Variation analysis to calculate D during the transition from classical to quantum-mechanical conduction. As T and A were adjusted to suppress the semi-classical process, the most anticipated scenario for the evolution of FCF towards a non-fractal trace was the one illustrated in Fig. 16(a) - the value of D was expected to remain constant whilst the range of ΔB over which fractal behavior was observed decreased to zero.[16, 50] In other words, the transition would be marked by a gradual deterioration in fractal observation, shifting the lower cut-off towards the higher cut-off, until the fractal scaling disappeared altogether. For example, consider raising T to induce the transition to the classical regime. In the traditional semi-classical picture, the ΔB spectrum of conductance fluctuations is directly related to the distribution of areas enclosed by classical trajectories (for a given trajectory, the Aharonov-Bohm effect predicts ΔB to be inversely proportional to the enclosed area).[14] Increasing T renders the longer trajectories incoherent, preventing the loops with the largest enclosed areas from contributing to the

FCF process. Thus the fluctuations with small ΔB should be suppressed first, leaving the large ΔB fluctuations relatively unaffected, as indicated in Fig. 16(a). Similarly, in the semi-classical to quantum transition, the deterioration in FCF behavior is predicted to set in when the semi-classical theory becomes invalid. This occurs when the electron states inside the billiard start to become resolved (as determined by the Heisenberg time, $\tau_H = m^*A/h$, where m^* is the electron effective mass).* As the billiard area is made smaller and consequently τ_H also becomes smaller, loops with traversal times longer than τ_H will no longer contribute to the semi-classical process.[16, 50, 53, 54] According to the Aharonov-Bohm effect, these longer loops correspond to small ΔB values. Thus, as indicated in Fig. 16(a), during the transition to fully quantum behavior, the fluctuations with small ΔB should be suppressed first, leaving the large ΔB fluctuations relatively unaffected.

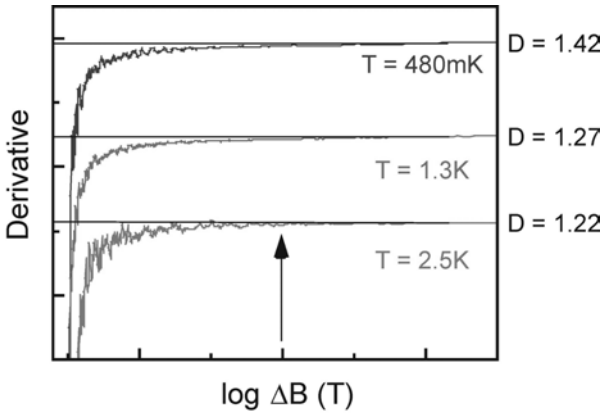

Figure 17 Derivative of –log N versus log ΔB for three temperatures (480mK, 1.3K and 2.5K) showing that the lower cut-off (indicated by the arrow) remains constant but D changes as a function of temperature.

In sharp contrast to these expectations, the fractal analysis revealed a more remarkable behavior, illustrated in Fig. 16(b), where the value of D decreased *gradually* towards the non-fractal value of 1 in both the classical and quantum limits![55] Due to its increased sensitivity to small changes, we demonstrate this behavior using the derivative technique introduced in Fig. 11(a). The derivative plot of Fig. 17 shows the effect of

* The billiard's average energy level spacing ΔE_S is calculated by dividing the energy of the highest occupied level (the Fermi energy) by the total number of occupied energy levels and this equals $2\pi\hbar^2/m^*A$ (see reference 54). By definition, the Heisenberg time is then given by $\tau_H = \hbar/\Delta E_S$ (see references 16, 50, 54).

changing T. In this figure, the D values (measured for the data of Fig. 15) are labelled next to the respective traces. The key observation is that the fractals turned out to be remarkably robust to deviations from the semi-classical regime. The fluctuations did *not* lose their fractal character (as defined by their fractional D value) as long as fluctuations could be observed. Rather than the expected deterioration (Fig. 16(a)), a smooth evolution in the fractal scaling properties was observed (Fig. 16(b)), involving an evolution of the entire ΔB spectrum.[53, 55]

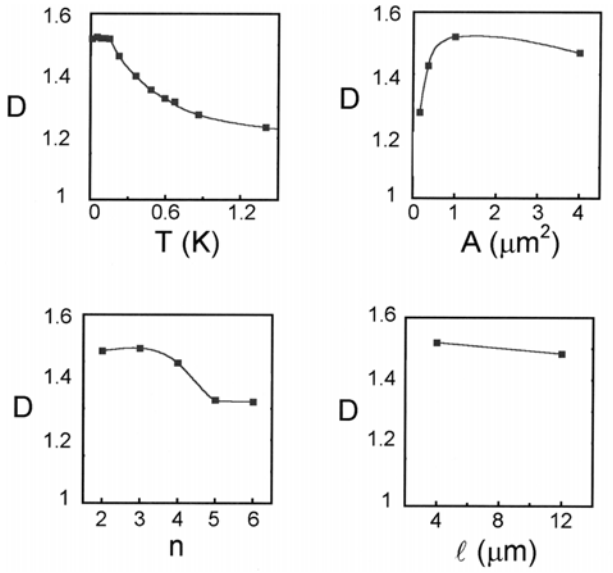

Figure 18 D plotted against T, A, n and ℓ. (A = 1μm^2, n = 2, ℓ = 4.4μm) for the T plot, (T = 30mK, n = 2, ℓ = 4.4μm) for the A plot, (T = 30mK, A = 1μm^2, ℓ = 4.4μm) for the n plot and (T = 30mK, A = 1μm^2, n = 2) for the ℓ plot.

To further confirm this unusual behavior, we next considered *all* four adjustable experimental parameters (T, A, n and ℓ) for the seven billiards presented in Fig. 14 and Table 1. As demonstrated in Fig. 18, the plots of D versus T, A, n and ℓ were all found to have different forms. However, we found that D changed in a *universal* way when plotted against a more general parameter Q that quantifies the transition towards resolvable, quantised energy levels within the billiard. We define Q as the ratio of the average energy level spacing ΔE_S to the average energy level broadening ΔE_B. The condition $Q = 0$ therefore corresponds to $\Delta E_S = 0$ or $\Delta E_B = \infty$. Q can then be increased either by increasing ΔE_S or decreasing ΔE_B, improving the resolution of the discrete energy levels. We calculate ΔE_S to equal $2\pi\hbar^2/m^*A$ (see footnote, page 32). ΔE_B is

given by the quadrature summation of the billiard's two characteristic energy broadening widths - thermal broadening kT and the intrinsic energy level broadening $\hbar/\tau_q$ originating from phase-breaking scattering events that limit the lifetime τ_q of the quantum states.* Thus:

$$Q = \frac{\Delta E_S}{\Delta E_B} = \frac{\left(2\pi\hbar^2\right)/\left(m^* A\right)}{\sqrt{(\hbar/\tau_q)^2 + (kT)^2}} \tag{4}$$

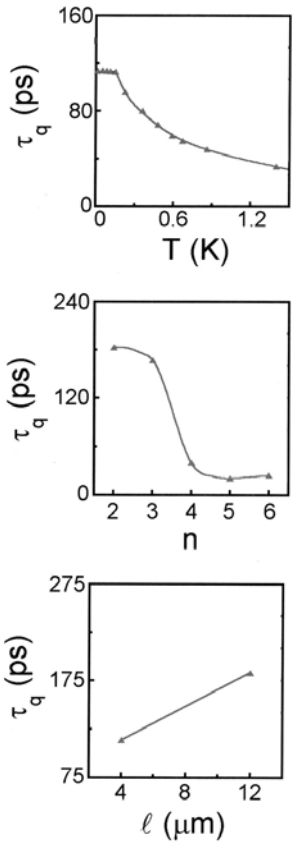

Figure 19 τ_q plotted against T, n and ℓ. (A = 1μm^2, n = 2, ℓ = 4.4μm) for the T plot, (T = 30mK, A = 1μm^2, ℓ = 4.4μm) for the n plot and (T = 30mK, A = 1μm^2, n = 2) for the ℓ plot.

To extract τ_q from the data, we used a well-established technique, commonly applied in semiconductor billiards, that analyses the correlation field of the data as a function of magnetic field.[57] In Fig. 19(a,b,c), we demonstrate how τ_q was varied using

* Guided by the Boltzmann picture of conductance, we determine ΔE_B from a convolution of the two energy broadening distributions – the scattering-broadened density of states and the derivative of the Fermi-Dirac function (see reference 56). We find that, for the parameter ranges considered, ΔE_B can be most closely approximated by the quadrature summation of the two characteristic widths kT and $\hbar/\tau_q$.

the experimental parameters. Reducing T induced the rise in τ_q shown in Fig. 19(a). The saturation at low T is a common observation in semiconductor billiards[54, 55, 57, 58] and in our experiments coincided with the condition $kT < \Delta E_S$. In Fig. 19(b), the gate bias V_g has been tuned in order to change n. We found that τ_q decreased for larger values of n due to an increased coupling to the external 2DEG environment.[53, 57, 58] We also varied ℓ by constructing billiards using different quality materials and found that τ_q scaled with ℓ (Fig. 19(c)). In addition to varying ΔE_B through changes in τ_q and T, we also varied ΔE_S through changes in A. To investigate a large range of A values, we constructed billiards with different physical areas. Tuning V_g was also used to change A. In particular, the side-gate featured in billiard d (see Fig. 14) could be used to reduce A to less than 20% of the physical area enclosed by the gates. Thus, in summary, we varied Q using all four available billiard parameters: T, A, n and ℓ. Table 1 shows the ranges of Q achieved.

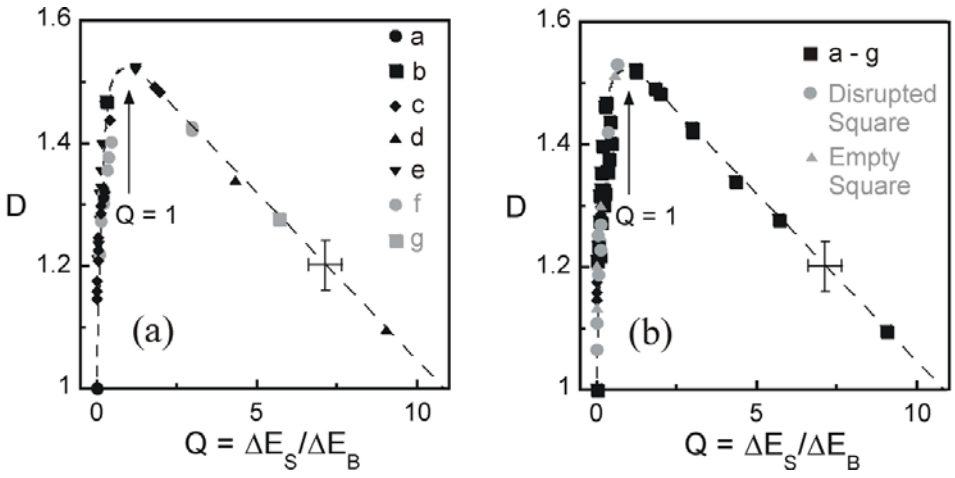

Figure 20 'Q curves' generated by plotting D against Q. (a) The Q curve for the original seven single-layer billiards, labelled a to g. The error bars indicate the largest possible uncertainties in D and Q. (b) The D values of the empty square and disrupted square are plotted against Q along with the original seven billiards (a to g). The dashes are guides to the eye.

In Fig. 20(a), all of the D measurements from the seven different billiards are plotted against Q. In contrast to the distinct forms of the D variations shown in Fig. 18, all of the D data condense onto a single 'universal' curve when plotted as a function of Q.[53] Therefore it is clear that Q, which gives a measure of how well the energy levels of the billiard are resolved, is a particularly useful parameter for charting the variations in D. Moving from left to right across Fig. 20(a), D rises and then falls. This trend can be

seen in the raw FCF data by moving down through Fig. 15. In the extreme limit of Q = 0, D assumes the non-fractal value of 1. As Q is increased, D rises smoothly until it reaches a peak value of 1.52 at Q = 1. Further increases in Q are accompanied by a gradual decrease in D. Extrapolating the downward trend in D, we find that to obtain D = 1 would require Q = 11. By this stage, the billiard width matches that of the openings and the device resembles a long channel.

It is important to emphasise that Q is an empirical parameter, identified from experiments rather than based on theory. Q is distinctly different to S, the parameter traditionally associated with theories charting evolutions in the semi-classical nature of a system. As discussed in the Introduction, S is the ratio of the billiard size to the electrons' Fermi wavelength. A large S value corresponds to fitting a large number of wavelengths along a typical trajectory – a necessary condition for most semi-classical models.* Whereas S is related to the ratio of Fermi energy to the energy level spacing, Q is the ratio of energy level spacing to energy level broadening. Thus, billiard parameters which alter the energy broadening (e.g. τ_q and T) can be used to alter Q whilst leaving S unaffected. Similarly, parameters that alter the Fermi energy can be used to alter S whilst leaving Q unaffected.† This difference in their dependences on billiard parameters can be used to establish that that Q rather than S is indeed the relevant parameter for charting the evolutions in D shown in Fig. 20(a). For example, billiards with the same Q values but substantially different S values have the same measured D values. However, data points with the same S values but different Q values have different measured D values. Having established that Q is the relevant parameter for charting the evolutions in D, in the next section we will discuss some unusual and surprising consequences of this result.

---

* It is relatively easy to show that S is inversely proportional to the effective Planck's constant of the system. A necessary condition of semi-classical pictures is that the effective $\hbar$ must be significantly smaller than $\hbar$ (see reference 16).

† Electron density is the parameter most commonly used to change the Fermi energy. Adjustments of electron density will therefore lead to direct changes in S. Note, however, that changes in electron density also indirectly affect Q - electron density alters the screening properties of the 2DEG, leading to changes in τ_q and thus ΔE_B.

Figure 21 A scanning electron micrograph of two surface gate patterns deposited on the same heterostructure, used to demonstrate that radically different billiard geometries generate the same *Q* curve. The square pattern is 1μm across.

7. The Role Played by the Billiard Walls

A central characteristic of the ballistic scattering regime is that the device walls play the dominant role over material-related scattering in determining the device conduction processes. The expectation is that geometry-related factors such as billiard shape and positioning of the entrance and exit should have a profound influence on quantum interference effects such as FCF. The results represented in the '*Q* curve' of Fig.20(a) stand in contradiction to this picture. Different billiard shapes and orientations of the openings were purposely used for the billiards examined (see Fig. 14). Yet Fig. 20(a) demonstrates that these factors do not influence *D*. For example, the bottom gate of device *d* (see Fig. 14) not only changes *A* but also the billiard's shape from that of a square to a thin rectangle, yet the induced evolution in *D* is well-charted by *Q* - a parameter which is insensitive to billiard shape. According to the Q curve, two billiards with radically different geometries will generate identical *D* values provided *Q* is set to be the same. To emphasise this result we examined the two billiards shown in Fig. 21. The two billiards were defined within one micrometre of each other on the same AlGaAs/GaAs heterostructure to ensure that they were described by identical material-related parameters. The only difference, therefore, between the two devices is the geometry – in particular, the finger-shaped extension incorporated into the gate design of the right-hand billiard. By raising the temperature to 4K to remove quantum interference effects, the classical magneto-conductance of each billiard was measured. As expected, the finger extension radically altered the distribution of the classical trajectories, leading to very different traces. Furthermore, when the devices were cooled to 20mk and the

FCF emerged on top of the classical background, there were clear differences in the individual features of the two sets of fluctuations. However, the statistics of the two FCF traces, as charted with D, were found to be identical. This is demonstrated in Fig 20(b), where the data for both devices condense onto the *same* 'Q curve.'

If the shape of the walls doesn't influence the fractal properties, perhaps the potential profile of the walls isn't important either? This defines a critical question in our investigations because the soft character of the profile is known to generate the mixed stable-chaotic trajectories believed to produce the FCF. More specifically, D is predicted to have a critical sensitivity to the *precise* profile.[16, 50] To investigate this FCF dependence on profile, we designed a unique 'double-layer' billiard system in which a common set of surface-gates define billiards in two 2DEGs located at different depths beneath the heterostructure surface. Using the procedure outlined below, the two billiards have nominally identical geometries but different soft-wall profiles, making them an ideal system for studying the relationship between quantum interference phenomena and wall profile.

The soft-wall profile of billiards is known to be sensitive to both surface-gate bias V_g and 2DEG depth z.[59, 60] Previously, FCF were investigated as a function of V_g due to the simplicity of adjusting V_g compared to z.[50] However, adjustments to V_g also modify A and n, both of which are known from the previous section to induce independent changes in the FCF. This obscures the relationship between the profile and the measured FCF. The 'double-layer' billiard was designed to overcome this problem. Figure 22(a) shows the device, which used a common set of surface gates to define billiards in 'shallow' (z = 90 nm) and 'deep' (z = 140 nm) 2DEGs. Note that the previous billiards examined in Section 6 (see Fig. 14 and Table 1) were defined in shallow 2DEGs. Fabrication details (including the 'isolation' gate technique that allowed the upper and lower 2DEGs to be measured separately) are discussed elsewhere.[61] Prior to activating the billiard gates, we matched the electron densities of the two 2DEGs by adjusting the bias applied to a back-gate.[61] The matched electron densities were $2.85\times10^{15}\mathrm{m}^{-2}$ (corresponding to a matched

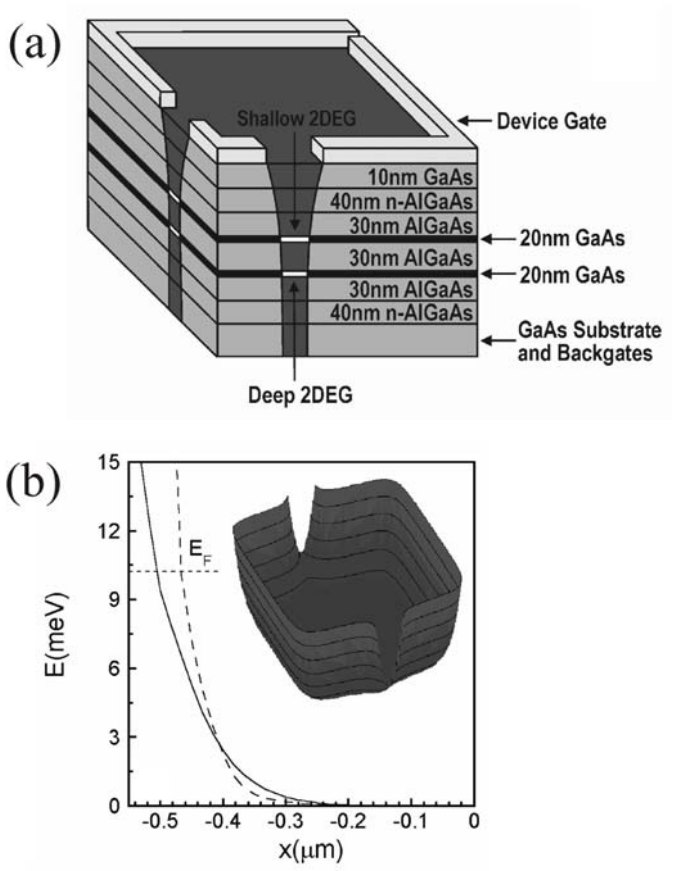

Figure 22 (a) A schematic representation of the double-layer AlGaAs/GaAs heterostructure system in which a common set of gates are used to define billiards in the 'shallow' and 'deep' 2DEGs. (b) (Inset) The confining potential of a soft-wall billiard. The potential energy (plotted vertically) has an approximately parabolic profile (plotted against spatial location) at the billiard edges and a flat bottom in the central region of the billiard. (b) (Main) Self-consistent profile models for the shallow (solid line) and deep (dashed line) billiards with $n = 6$. Energy E is plotted against spatial location x, where $x = 0$ corresponds to the center of the billiard. A 16% difference is predicted for the areas of the two billiards.

E_F of 10.2meV and a Fermi wavelength of 50nm) and the electron mobilities in the shallow and deep 2DEGs were 130 and 110 m^2/Vs respectively (corresponding to ℓ values of 12μm and 10μm respectively).

Because of the 50nm separation between the 2DEGs, electron tunnelling and interaction effects were expected to be negligible.[62, 63] In Fig. 23(a), the shallow billiard is shown to exhibit *identical D* behavior to the shallow billiards in single-layer systems, confirming that the FCF are not affected by coupling effects between the shallow and deep billiards. We now describe the procedure for measuring the FCF shown in Fig. 24(b). First, the deep 2DEG was electrically disconnected from the measurement circuit

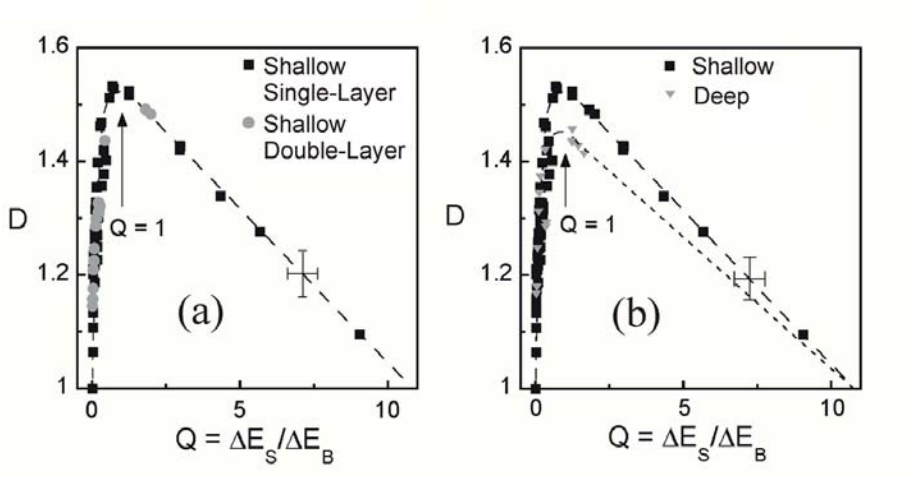

Figure 23 '*Q* curves' generated by plotting *D* against *Q*. (a) The *D* values for the shallow double-layer billiard are plotted against *Q,* along side the *D* values for the nine single-layer billiards of Fig. 20(b). (b) The *D* values of the deep billiard are compared to the *D* values shown in (a).

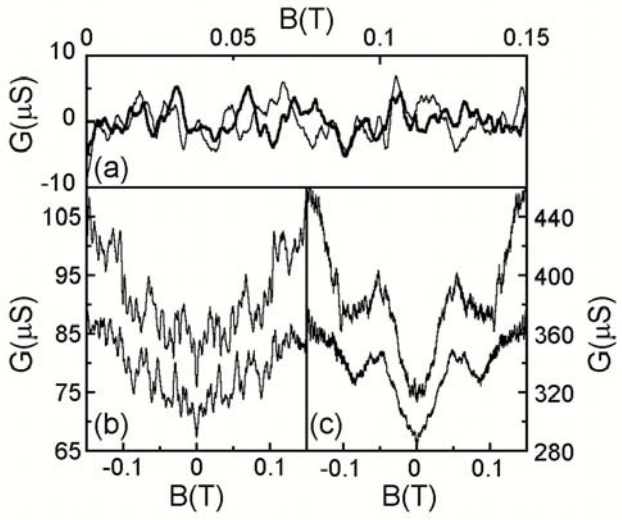

Figure 24 (a) An overlay of FCF traces (with classical backgrounds removed and for $B > 0$ only) from the deep and shallow billiards for $n = 2$. *G(B)* traces for the shallow (upper traces) and deep (lower traces) billiards at (b) $n = 2$ and (c) $n = 8$. The shallow billiard traces are offset by 20μS and 5μS respectively for clarity. For all traces $T = 20$mK.

(using the isolation gates)[61] in order to measure just the shallow billiard. The biases of the three billiard surface gates (see Fig. 22(a)) were then individually tuned to form a billiard in the shallow 2DEG with $n = 2$ and the FCF for this shallow billiard were then measured (upper trace of Fig. 24(b)). The shallow 2DEG was then disconnected and the three gate biases were re-tuned to form a billiard in the deep 2DEG with $n = 2$ and the FCF for this deep billiard were measured (lower trace of Fig. 24(b)). Using this technique, the two billiards (shallow and deep) were independently measured for

identical n values and had A values (measured using the high field Aharonov-Bohm effect)[7] matched to within 14%, a difference that previous studies (Section 6) indicated will produce less than a 1% change in D.

In terms of geometry (n, A and gate shape), the two billiards were, therefore, essentially matched. Crucially, however, the shallow billiard profile was softer than that of the deep billiard due to the smaller V_g required to define it.[64] The profiles, calculated using self-consistent numerical simulations, are shown in Fig. 22(b). The profile gradient P at E_F differs by a factor of three between the two billiards. Note also that the difference in profile is not limited to the edge of the billiard. Fig. 22(b) shows that the two profiles differ by at least 0.5meV (corresponding to 5% of E_F) across more than a quarter of the width of the billiard. Given the predicted critical sensitivity to profile,[16, 50] this is expected to significantly re-distribute the classical trajectories. Our double-layer billiard strategy of using a common set of surface gates offers significant advantages over other possible approaches to this experiment. One alternative approach, adopted in Ref. 50, simply uses the changes in V_g applied to a single-layer billiard to induce variations in P. However, this does not allow independent control of n and P: for example, our simulations show that a change in P of only a factor of two is accompanied by a change in n from 2 to 6. Another approach would be to use two single-layer billiards of different lithographic sizes and to apply different V_g to the two billiards to induce the same A and n but differing P. However, this approach introduces problems associated with lithographic variations in the two sets of gate patterns defining the two billiards and, since the mixed electron dynamics are extremely sensitive to the precise billiard geometry,[16, 50] this is not desirable.

Magneto-conductance $G(B)$ traces measured at T = 20mK are shown in Fig. 24(b,c) and reveal FCF superimposed on a classical background. For each of the two n settings, the similarity between the classical structure of the deep and shallow billiards confirms that both have the same nominal geometry (i.e. size and shape). To better compare the actual FCF, in Fig. 24(a) we present an overlay of the traces in Fig. 24(b) with their classical backgrounds removed. It is evident that the differing wall profile induces a significant change in the precise details of the FCF, and intuitively, one might

expect that the fractal scaling has changed, as predicted by theory.[16, 50] We investigated the effect of the change in profile on two FCF parameters – the ΔB range over which fractal scaling was observed and D. The locations of the upper and lower limits of fractal scaling matched for the two billiards, and this is expected since neither limit is related to the soft-wall profile (see Section 5). In Fig. 23(b), the Q curve obtained for the deep billiard is compared to that of the shallow billiards. In the regime $Q < 1$, the D values for the deep and shallow billiards agree within experimental uncertainties. In other words, although the difference in billiard profile is sufficient to induce changes in the individual features of the FCF, the statistical characteristics of the FCF have not changed. At $Q = 1$, the D values obtained for the deep billiard (with the harder profile) are lower than those measured for the shallow billiards. This raises the possibility that the deep billiard is following a slightly different Q curve and that this difference might persist in the fully quantum regime of $Q > 1$ (the dashed line indicates a possible scenario for the second Q curve). Although technically challenging, we plan to investigate smaller sized billiards to compare deep and shallow billiards in the $Q > 1$ regime.

8. Conclusions

In this chapter, we have reviewed our experimental investigations of the fractal behavior observed in the low temperature magneto-conductance of semiconductor billiards. We found that the fractal properties could be detected over scaling ranges of up to 3.7 orders of magnitude in ΔB - substantially larger than the observational ranges of typical physical systems. As a consequence, we were able to determine the parameters that quantify the fractal properties (such as the fractal dimension D and similarity correlation F) with great accuracy. We showed that the billiards could be used to induce two distinct forms of fractals - exact and statistical self-affinity. We exploited the high degree of control provided by the electrostatic gate technique to study the experimental conditions for which each form of fractals is observed. Because this existence of two forms of fractals in one physical system is rare, these experiments provided a unique environment in which the fundamental evolution in fractal form could be studied.

Having noted the scientific appeal of semiconductor billiards as a physical system in which to study fractal phenomena, the subtlety of the relationship between the fractal conductance and the dynamics of the electrons should also be stressed – after over five years of investigation, there is no theoretical framework that can fully explain the observed properties of either the exact or statistical self-affinity. The generation of exact self-affinity using the central 'plunger' gate of the Sinai billiard (see Fig. 3) is linked to the formation of a scattering region at the billiard's center. However, this central scatterer does not act as a Sinai diffuser, as originally intended. According to Sinai's theory, the Sinai diffuser would have had the same effect on the billiard's dynamics if the curved surface had been incorporated into the billiard side-wall rather than at the center. Yet device *d* (see Fig. 14), which features a curved side-gate, generates statistical rather than exact self-affinity. This confirms that the role of the circular gate in Fig. 3 is more subtle than simply introducing a curved surface into the billiard's geometry - its insertion *at the billiard's center* is crucial for the generation of exact self-affinity. Due to the complexity of the mixed chaotic-stable trajectory system revealed in the Poincaré plots, the plunger gate's action on individual trajectories is not fully understood. However, from the discussions of Section 4, it is clear that the central scatterer acts as a 'trajectory selector'.* Removal of the scatterer introduces extra sets of trajectories into the billiard, which together with the original trajectories, lead to the observed statistical self-affinity.

This statistical self-affinity appears to be a generic property of 'empty' billiards. The evolution in statistical self-affinity charted by the Q curve extends across a remarkably comprehensive range of billiard conditions. In particular, in following the Q curve, the fractal behavior persists well beyond the specific conditions required by existing semi-classical theory, which links the fractal fluctuations to the areas enclosed by the classical trajectories.[16, 50] The region of the Q curve where the semi-classical theory *is* valid centers around $Q = 1$ (in this region both τ_q and S are sufficiently large for the semi-classical theory to hold), where the curve peaks at $D = 1.52$. Significantly, this peak

* This picture is in agreement with recent theoretical investigations that reproduced the exact self-affinity (see reference 65). In this theory the selected trajectories generating the exact self-affinity are a set of self-similar unstable periodic orbits.

value of 1.52 matches the maximum value predicted by the semi-classical theory. Therefore, across this narrow range of the Q curve, the experimental observations match the semi-classical predictions for D. However, the manner in which D evolves on moving away from the Q = 1 region reveals dramatic discrepancies between the experiment and the predictions of the semi-classical theory. According to the semi-classical theory, the mixed chaotic-stable system of classical trajectories features a power-law distribution of loop areas and D is directly related to the exponent γ of this distribution according to the expression $D = 2 - (\gamma / 2)$ (see Section 5). Crucially, D should therefore depend only on parameters that affect γ through re-arrangements of the loop distribution. According to this theory, D should not depend on temperature T or parameters that determine τ_q. However, this central prediction is *not* in agreement with the experimental observations, where D depends on both T and τ_q through Q (see Equation 4). Again in conflict with our experiments, the dependence on A is predicted by the semi-classical theory to be erratic since it will lead to trajectories with different classical power-law exponents. However, the experimental observations charted by Equation 4 reveal a smooth, well-defined evolution of D as a function of A. In addition to contradicting the original semi-classical predictions, Equation 4 also stands in contrast to more recent semi-classical modelling predicting that, instead of depending on Q, D should depend on the ratio of the width of the openings to that of the billiard.[66] In summary, although the semi-classical picture leads to an elegant explanation for how fractals might be generated by a semiconductor billiard, it fails to explain essential characteristics of the observed FCF, suggesting that a very different process is responsible.

It is worth emphasizing that our experimental findings are not just in conflict with existing theory but, more generally, with what one might have expected intuitively. In the past, a simple semi-classical picture of electron transport has been found to be an extremely powerful tool for the intuitive understanding of the ΔB spectrum of quantum conductance fluctuations in ballistic cavities. The results presented in Fig. 20 thus raise questions, not only regarding the physical origin of FCF, but also more fundamentally about our understanding of ballistic quantum transport. As discussed in relation to Fig.

20 (see Section 6), the observed gradual change in D is in sharp contrast to expectations based on the Aharonov-Bohm effect - it indicates that the whole ΔB spectrum is evolving with temperature, otherwise the fractal scaling relationship could not be preserved. The Q curve of Fig. 20 predicts further counter-intuitive behavior. Starting at low temperatures (high Q in Fig. 20), the Q curve predicts that a rise in temperature will be accompanied by a rise in D, indicating that the contributions of the large ΔB (small area) fluctuations are suppressed more rapidly than the small ΔB (large areas) fluctuations. This is again in contradiction to expectations based on the Aharanov-Bohm effect. These unusual trends have no simple explanation! What is clear, however, is that the resolution of electron states, as described by the empirical parameter Q, is central to the evolution process. Furthermore, in identifying Q, we emphasize that D is determined only by conditions *within* the billiard rather than the electron injection properties. Billiard opening parameters, such as n, only affect D indirectly through their effect on τ_q and therefore Q.

More recently, a number of theoretical papers have started to explore beyond the original semi-classical theory of mixed dynamics.[67-71] However, in general, modifications to the original theory predict the appearance of individual resonances in the conductance fluctuations rather than the evolution in fractal behavior charted by the Q curve. In particular, why the fractal behavior persists into the fully quantum regime of conduction remains a mystery. Whereas a theory for fractal fluctuations in the fully quantum regime has been published[70] this was developed for the case of strong localization and therefore is not applicable to our billiards. At the present stage of our understanding of FCF, where theoretical and experimental results are inconsistent, it is critical to identify parameters that are accessible to both theory and experiment. Current and future experiments feature two complementary lines of investigation, each of which addresses one such parameter.

Specifically, we are studying the two fundamental processes of ballistic transport: the mechanism by which the electrons are injected into the ballistic device and the

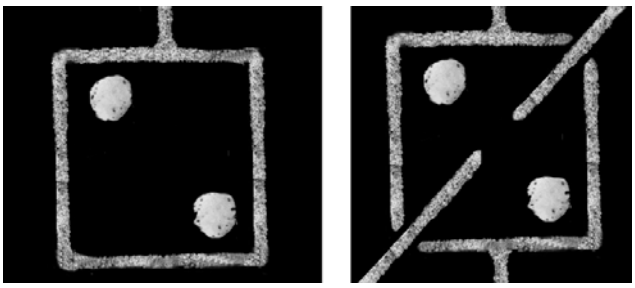

Figure 25 Schematic representations of future billiard designs in which Ohmic spikes (circular metallic patterns) will be used to inject electrons directly into the confined regions of billiards defined by surface gates (grainy patterns).

manner in which they interact with the device walls. In the first study, electrons will be injected directly into the middle of the billiard rather than through entrances in the walls.[72] This technique uses the phase-coherent sub-micron ohmic contacts shown in Fig. 25. Electrons injected from the contacts will allow the study of quantum phenomena such as FCF of an 'isolated' billiard (i.e. a billiard which is no longer linked to the outside 2DEG environment via openings). This is a very different approach to 'closed' billiard studies than those carried out by closing the wall openings, where electron conduction enters the tunneling regime. The central aim is to determine if the generic fractal character of quantum conduction extends to this new form of semiconductor billiard. The second study builds on our investigations of wall profile discussed in Section 7. In addition to using the double-layer billiard to define billiards of varying softness, we are investigating billiards defined in InGaAs/InP heterostructures. Simulations for these devices indicate that the walls have hard profiles and these experiments will therefore determine whether softness is necessary for the generation of the FCF. We note that preliminary investigations of InGaAs/InP billiards indicate that magneto-conductance fluctuations are fractal and that their D values condense onto the same Q curve as AlGaAs/GaAs billiards, further emphasising the generic character of this remarkable phenomenon.

Acknowledgments: The authors thank A. Sachrajda, P. Coleridge, Y. Feng, M. Pepper, C. Dettmann, J. Cooper, D. Ferry, Y. Aoyagi, T. Sugano, L. Macks, B. Tribe, E. Linfield, D. Ritchie, A. Ehlert, I. Shorubalko, P. Omling, C. Tench and P. Wilkinson for their valued assistance.

References

[1] R. P. Taylor, The Role of Surface Gate Technology for ALGaAs/GaAs Nanostructures, *Journal of Nanotechnology* **5,** 183 (1994).

[2] *Microstructural Engineering*, edited by R. P. Kramer (Delft University Press, Amsterdam, 1981), pp. 381, and *The Physics and Fabrication of Microstructures and Microdevices*, edited by M. J. Kelly and C. Weisbuch (Springer-Verlag, Berlin, 1986), pp. 36.

[3] H. G. Craighead, A. Scherer, and M. L. Roukes, *Nanofabrication* in: *The Physics and Technology of Submicron Structures*, edited by Heinrich, Bauer, and Kuchar (Springer, Heidelberg, 1988).

[4] T. J. Thornton, M. Pepper, H. Ahmed, D. Andrews, and G. J. Davies, One-Dimensional Conduction in the 2D Electron Gas of a GaAs-AlGaAs Heterojunction, *Physcal Review Letters* **56**, 1198-1201 (1986).

[5] B. J. van Wees, H. van Houten, C. W. J. Beenakker, J. G. Williamson, L. P. Kouwenhoven, D. van der Marel, and C. T. Foxon, Quantized Conductance of Point Contacts in a Two-Dimensional Electron Gas, *Physical Review Letters* **60**, 848-51 (1988).

[6] D. A. Wharam, T. J. Thornton, R. Newbury, M. Pepper, H. Ahmed, J. E. F. Frost, D. G. Hasko, D. C. Peacock, D. A. Ritchie, and G. A. C. Jones, One-Dimensional Transport and the Quantisation of the Ballistic Resistance, *Journal of Physics C* **21**, L209-212 (1988).

[7] C. W. J. Beenakker and Van H. Houten, Quantum Transport in Semiconductor Nnaostructures, *Solid State Physics* **44,** 1 (1991).

[8] C. M. Marcus, A. J. Rimberg, R. M. Westervelt, P. F. Hopkins, and A. C. Gossard, Conductance Fluctuations and Chaotic Scattering in Ballistic Microstructures, *Physical Review Letters* **69**, 506-509 (1992).

[9] A. M. Chang, H. U. Baranger, L. N. Pfeiffer, and K. W. West, Weak Localization in Chaotic versus Nonchaotic Cavities: a Striking Difference in the Line Shape, *Physical Review Letters* **73,** 2111-2114 (1994).

[10] R. A. Jalabert, H. U. Baranger, and A. D. Stone, Conductance Fluctuations in the Ballistic Regime: a Probe of Quantum Chaos?, *Physical Review Letters* **63,** 2442-2445 (1990).

[11] H. U. Baranger, R. A. Jalabert, and A. D. Stone, Weak Localisation and Instability in Ballistic Cavities, *Physical Review Letters* **70,** 3876-3879 (1993).

[12] E. Ott, *Chaos in Dynamical Systems* (Cambridge University Press, Cambridge, 1993).

[13] For a review see K. Nakamura, *Quantum Chaos – A New Paradigm of Non-linear Dynamics* (Cambridge Universty Press, Cambridge, 1993).

[14] Y. Aharonov and D. Bohm, Significance of Electromagnetic Potentials in the Quantum Theory, *Physical Review* **115,** 485 (1959).

[15] R. P. Taylor, P. C. Main, L. Eaves, S. Thoms, S. P. Beaumont, and C. D. W. Wilkinson, Universal Conductance Fluctuations in the Magnetoresistance of Submicron-Size GaAs Wires, *Surface Science* **196,** 52-55 (1988).

[16] R. Ketzmerick, Fractal Conductance Fluctuations in Generic Chaotic Cavities, *Physical Review B* **54,** 10841-10844 (1996).

[17] B. B. Mandelbrot, *The Fractal Geometry of Nature* (Freeman and Company, New York, 1977).

[18] J.-F. Gouyet, *Physics and Fractal Structures* (Springer-Verlag, New York, 1996).

[19] R. P. Taylor, R. Newbury, R. B. Dunford, P. T. Coleridge, A. S. Sachrajda, and J. A. Adams, A Tunable Ballistic Electron Cavity Exhibiting Geometry Induced Weak Localization, *Superlattices and Microstructures* **16,** 317 (1994), R. P. Taylor, R. Newbury, R. B. Dunford, P. T. Coleridge, A. S. Sachrajda, and J. A. Adams, Classical and Weak Localization Processes in a Tunable Ballistic Electron Cavity, *Physical Review B* **51,** 9801 (1995), and R. P. Taylor, R. Newbury, A. S. Sachrajda, P. T. Coleridge, P. Zawadzki, R. B. Dunford, Y. Feng, J. P. Bird, C. R. Leavens, J. M. Cadogan, J. A. Adams, P. J. Kelly, M. Davies, and S. Brown, The Use of Wide Ballistic Cavities to Investigate Local Weak Localization Processes Induced by Geometric Scattering, *Semiconductor Science and Technology* **11,** 1 (1996).

[20] Y. G. Sinai, Dynamical Systems with Elastic Reflections, *Russian Mathematical Surveys* **25,** 137 (1970).

[21] E. Doron, U. Smilansky, and A. Frenkel, Experimental Demonstration of Chaotic Scattering of Microwaves, *Physical Review Letters* **65,** 3072-3075 (1990).

[22] V. Milner, J. L. Hanssen, W. C. Campbell, and M. G. Raizen, Optical Billiards for Atoms, *Physical Review Letters* **86,** 1514-1517 (2001).

[23] A. Kaplan, N. Friedman, M. Anderson, N. Davidson, Observation of Islands of Stability in Soft Wall Atom-Optics Billiards, *Physical Review Letters* **87,** 274101-1-4 (2001).

[24] R. P. Taylor, R. Newbury, A. S. Sachrajda, Y. Feng, N. Zhu, H. Guo, P. T. Coleridge, A. Delage, P. J. Kelly, Z. Wasilewski, and P. Zawadski, Geometry-Induced Quantum Interference: a Continuous Evolution from Square to Sinai Billiard, *Superlattices and Microstructures* **20,** 297-305 (1996), and R. P. Taylor, R. Newbury, A. S. Sachrajda, Y. Feng, P. T. Coleridge, Z. Wasilewski, N. Zhu, and H. Guo, The Transition from a Square to a Sinai Billiard, in: *World Scientific* **2,** edited by M. Scheffler and R. Zimmermann, 1549-1552 (1996).

[25] R. P. Taylor, J. A. Adams, M. Davies, P. A. Marshall, and R. Barber, Fabrication of Nanostructures with Multi-level Architecture, *Journal of Vacuum Science and Technology B* **11,** 628 (1993).

[26] R. P. Taylor, Y. Feng, A. S. Sachrajda, J. A. Adams, and M. Davies, Fabrication and Characterization of Multi-level Lateral Nanostructures, *Surface Science* **305,** 648-651 (1994).

[27] R. Shaw, *The Dripping Faucet as a Model Chaotic System* (Aerial Press, Santa Cruz, 1984).

[28] R. P. Taylor, A. P. Micolich, R. Newbury, C. Dettmann, and T. M. Fromhold, Fractal Transistors, *Semiconductor Science and Technology* **12,** 1459-1464 (1997).

[29] T. M. Fromhold, Fractal Resistance in a Transistor, *Nature* **386,** 124 (1997).

[30] R. P. Taylor, R. Newbury, A. S. Sachrajda, Y. Feng, P. T. Coleridge, C. Dettmann, N. Zhu, H. Guo, A. Delage, P. J. Kelly, and Z. Wasilewski, Self-Similar Magnetoresistance in a Semiconductor Sinai Billiard, *Physical Review Letters* **78,** 1952-1955 (1997).

[31] R. P. Taylor, R. Newbury, A. S. Sachrajda, Y. Feng, and P. T. Coleridge, Tunable Semiconductor Sinai Billiards, IEEE Journal [ISBN 0-7803-3374-8/97] (1997)**,** pp. 171-173.

[32] R. P. Taylor, A. P. Micolich, R. Newbury, and T. M. Fromhold, Correlation Analysis of Self-Similarity in Semiconductor Billiards, *Physical Review B Rapid Communication* **56,** R12733-R12756 (1997).

[33] R. P. Taylor, A. P. Micolich, R. Newbury, J. P. Bird, T. M. Fromhold, J. Cooper, Y. Aoyagi, and T. Sugano, Exact and Statistical Self-Similarity in Semiconductor Billiards: a Unified Picture, *Physical Review B* **58,** 11107-11110 (1998).

[34] R. P. Taylor, A. P. Micolich, R. Newbury, T. M. Fromhold, and C. R. Tench, Observation of Fractal Conductance Fluctuations over Three Orders of Magnitude, *Australian Journal of Physics* **52,** 887-893 (1999).

[35] R. P. Taylor, A. P. Micolich, R. Newbury, T. M. Fromhold, A. Ehlert, A. G. Davies, C. R. Tench, J. P. Bird, H. Linke, W. R. Tribe, E. H. Linfield, and D. A. Ritchie, Semiconductor Billiards: a Controlled Environment to Study Fractals, in: *Nobel Symposium on Quantum Chaos,* edited by K. F. Berggren and S. Aberg (World Scientific, Singapore [ISBN 981 02 4711-7], and The Royal Swedish Academy of Sciences, 2001) pp. 41-49.

[36] D. Avnir, O. Biham, and O. Malcai, Is the Geometry of Nature Fractal?, *Science* **279,** 39 (1998).

[37] See, for example, J. P. Bird, Recent Experimental Studies of Electron Transport in Open Quantum Dots, *Journal of Physics: Condensed Matter* **11,** R413 (1999).

[38] R.V. Jensen, The Signature of Chaos, *Chaos* **1,** 101 (1991).

[39] T. M. Fromhold, C. R. Tench, R. P. Taylor, A. P. Micolich, and R. Newbury, Self-Similar Conductance Fluctuations in a Sinai Billiard with Mixed Chaotic Phase Space: Theory and Experiment, *Physica B* **249-251,** 334-338 (1998).

[40] Y. Takagaki, and K. H. Ploog, Numerical Simulation of Fractal Conductance Fluctuations in Softwall Cavities, *Physical Review B* **61,** 4457-4461 (2000) and Relation Between Stable Orbits and Quantum Transmission Resonance in Ballistic Cavities, *Physical Review E* **62**, 4804-4808 (2000).

[41] A. P. Micolich, R. P. Taylor, R. Newbury, T. M. Fromhold, and C. R. Tench, The Weierstrass Function as a Model of Self-Similarity in a Semiconductor Sinai Billiard, *Europhysics Letters* **49,** 417-423 (2000).

[42] S. Kawabata and K. Nakamura, Altshuler Aronov Spivak Effect in Ballistic Chaotic Agharonov-Bohm Billiards, *Journal of the Physical Society of Japan* **65,** 3708 (1996).

[43] G. H. Hardy, *Transcripts of the American Mathematics Society* **17,** 301 (1916).

[44] A. P. Micolich, R. P. Taylor, J. P. Bird, R. Newbury, T. M. Fromhold, J. Cooper, Y. Aoyagi, and T. Sugano, Scale Factor Mapping of Statistical and Exact Self-Similarity in Billiards, *Semiconductor Science and Technology* **13,** A41-43 (1998).

[45] R. P. Taylor, Levy Flights, in: *Encyclopedia of Non-linear Science,* edited by Alywn Scott (to be published by Fitzroy-Dearborn, London, 2003).

[46] A. P. Micolich, R .P. Taylor, R. Newbury, J. P. Bird, R. Wirtz, C. P. Dettmann, Y. Aoyagi, and T. Sugano, Geometry Induced Fractal Behavior in a Semiconductor Billiard, *Journal of Physics: Condensed Matter* **10,** 1339-1347 (1998), and R. P. Taylor, A. P. Micolich, T. M. Fromhold, and R. Newbury, Comment on Fractal Conductance Fluctuations in a Soft Wall Stadium and a Sinai Billiard, *Physical Review Letters* **83,** 1074 (1999).

[47] A. P. Micolich, R. P. Taylor, J. P. Bird, and R. Newbury, Electron Behavior in AlGaAs/GaAs Square Quantum Dots, Proceedings of "The New Zealand and Australian Institutes of Physics Annual Condensed Matter Physics Meeting" [ISSN 1037-1214] (1997), pp. TP20.

[48] B. Dubuc, J. F. Quiniou, C. Roques-Carnes, C. Tricot, and S.W. Zucker, Evaluating the Fractal Dimension of Profiles, *Physical Review A* **39**, 1500 (1989).

[49] Y. Takagaki, M. ElHassan, A. Shailos, C. Prasad, J. P. Bird, D. K. Ferry, K. H. Ploog, L. H. Lin, N. Aoki, and Y. Ochiai, Magnetic Field Controlled Electron Dynamics in Quantum Cavities, *Physical Review B* **62,** 10255-10260 (2000).

[50] A. S. Sachrajda, R. Ketzmerick, C. Gould, Y. Feng, P. J. Kelly, A. Delage, and Z. Wasilewski, Fractal Conductance Fluctuations in a Softwall Stadium and a Sinai Billiard, *Physical Review Letters* **80,** 1948-1951 (1998).

[51] Y. Ochiai, L. H. Lin, K. Yamamoto, K. Ishibashi, Y. Aoyagi, T. Sugano, J. P. Bird, D. Vasileska, R. Akis, and D. K. Ferry, Low Temperature Magnetotransport in Ballistic Quantum Dots and Wires, *Semiconductor Science and Technology* **13,** A15 (1998).

[52] H. Hegger, B. Huckestein, K. Hecker, M. Janssen, A. Freimuth, G. Reckziegel, and R. Tuzinski, Fractal Conductance Fluctuations in Gold Nanowires, *Physical Review Letters* **77,** 3885-3888 (1996).

[53] A. P. Micolich, R. P. Taylor, A. G. Davies, J. P. Bird, R. Newbury, T. M. Fromhold, A. Ehlert, H. Linke, L. D. Macks, W. R. Tribe, E. H. Linfield, D. A. Ritchie, J. Cooper, Y. Aoyagi, and P. B. Wilkinson, Evolution of Fractal Patterns during a Classical-Quantum Transition, *Physical Review Letters* **87,** 036802-1-4 (2001).

[54] R. M. Clarke, I. H. Chan, C. M. Marcus, C. I. Duruoz, J. S. Harris, K. Campman, and A. C. Gossard, Temperature Dependence of Phase Breaking in Ballistic Quantum Dots, *Physical Review B* **52**, 2656 (1995).

[55] A. P. Micolich, R. P. Taylor, R. Newbury, J. P. Bird, Y. Aoyagi, and T. Sugano, Temperature Dependence of the Fractal Dimension of Magnetoconductance Fluctuations in a Mesoscopic Semiconductor Billiard, *Superlattices and Microstructures* **25,** 157-161 (1999).

[56] J. M. Ziman, *Electrons and Phonons; The Theory of Transport Phenomena in Solids* (Clarendon Press, Oxford, 1960).

[57] J. P. Bird, K. Ishibashi, D. K. Ferry, R. Newbury, D. M. Olatona, Y. Ochiai, Y. Aoyagi, and T. Sugano, Phase Breaking in Ballistic Quantum Dots: a Correlation Field Analysis, *Surface Science* **361/362**, 730-734 (1996).

[58] D. P. Pivin, A. Andresen, J. P. Bird, and D. K. Ferry, Saturation of Phase Breaking in an Open Ballistic Quantum Dot, *Physical Review Letters* **82**, 4687-4700 (1999).

[59] Y. Sun, G. Kirczenow, A. S. Sachrajda, and Y. Feng, An Electrostatic Model of Split-Gate Quantum Wires, *Journal of Applied Physics* **77,** 6361 (1995).

[60] O. E. Raichev and F. T. Vasko, Edge-Induced Modification of Tunnel Mixing and Resistance Resonance in Double-Quantum-Well Strips, *Physical Review B* **57,** 12350 (1998).

[61] A. P. Micolich, R. P. Taylor, A. G. Davies, T. M. Fromhold, H. Linke, R. Newbury, A. Elhert, L. D Macks, W. R. Tribe, E. H. Linfield, and D. A. Ritchie, Dependence of Fractal Conductance Fluctuations on Soft-Wall Profile in a Double-Layer Semiconductor Billiard, *Applied Physics Letters* **80,** 4381-4383 (2002).

[62] N. P. R. Hill, J. T. Nicholls, E. H. Linfield, M. Pepper, D. A. Ritchie, G. A. C. Jones, Y. K. H. Ben, and K. Flensberg, Correlation Effects on the Coupled Plasmon Modes of a Double Quantum Well, *Physical Review Letters* **78,** 2204-2207 (1997).

[63] T. J. Gramila, J. P. Eisenstein, A. H. Macdonald, L. N. Pfeiffer, and K. W. West, Mutual Friction Between Parallel Two-Dimensional Electron Systems, *Physical Review Letters* **66,** 1216-1219 (1991).

[64] K. J. Thomas, M. Y. Simmons, J. T. Nicholls, D. R. Mace, M. Pepper, and D. A. Ritchie, Ballistic Transport in One-Dimensional Constrictions Formed in Deep Two-Dimensional Electron Gases, *Applied Physics Letters* **67,** 109-111 (1995).

[65] A. Budiyono and K. Nakamura, Self-similar Magnetoconductance Fluctuations Induced by Self-Similar Periodic Orbits (submitted).

[66] E. Louis and J. A. Verges, Self-Similar Magnetoconductance Fluctuations in Quantum Dots, *Physical Review B* **61,** 13014-13020 (2000).

[67] B. Huckerstein, R. Ketzmerick, and C. H. Lewenkopf, Quantum Transport Through Ballistic Cavities: Soft vs Hard Quantum Chaos, *Physical Review Letters* **84,** 5504-5507 (2000).

[68] R. Ketzmerick, L. Hufnagel, F. Steinbach, and M. Weiss, New Class of Eigenstates in the Generic Hamiltonian Systems, *Physical Review Letters* **85,** 1214-1217 (2000).

[69] G. Casati, I. Guarneri, and G. Maspero, Frcatal Survival Probability Fluctuations, *Physical Review Letters* **84,** 63-66 (2000).

[70] G. Benenti, G. Casati, I. Guareri, and M. Terraneo, Quantum Fractal Fluctuations, *Physical Review Letters* **87,** 014101-1-4 (2001).

[71] A. P. S. de Moura, Y. C. Lai, R. Akis, J. P. Bird, and D. K. Ferry, Tunnelling and Nonhyperbolicity in Quantum Dots, *Physical Review Letters* **88,** 236804-1-4 (2002).

[72] R. P. Taylor, R. Newbury, A. S. Schrajda, Y. Feng, P. T. Coleridge, M. Davies, and J. P. McCaffrey, An Investigation of Current Injection Properties of Ohmic Spikes in Nanostructures, *Superlattices and Microstructures* **24**, 337-345 (1998) and Can Ohmic Spikes Define Quantum Systems?, *Japanese Journal of Applied Physics* **36,** 3964-3967 (1997).